AD-A281 053

ROME LABORATORY

FORMULATION OF PROBE-CORRECTED TIME-DOMAIN PLANAR NEAR-FIELD MEASUREMENTS

Thorkild B. Hansen, Arthur D. Yaghjian

DTIC
ELECTE
JUL 06 1994
S F D

Rome Laboratory
Air Force Materiel Command
Griffiss Air Force Base, New York

94-20530

DTIC QUALITY INSPECTED 3

94 7 5 200

This report has been reviewed by the Rome Laboratory Public Affairs Office (PA) and is releasable to the National Technical Information Service (NTIS). At NTIS it will be releasable to the general public, including foreign nations.
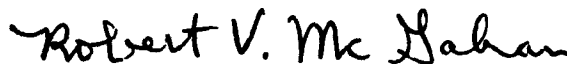
RL-TR-94-74 has been reviewed and is approved for publication.

APPROVED:

JOHN F. LENNON, Acting Chief
Applied Electromagnetics Division
Electromagnetics & Reliability Directorate

FOR THE COMMANDER:

ROBERT V. MCGAHAN
Acting Director
Electromagnetics & Reliability Directorate

If your address has changed or if you wish to be removed from the Rome Laboratory mailing list, or if the addressee is no longer employed by your organization, please notify RL(ERCT) Hanscom AFB MA 01731-3010. This will assist us in maintaining a current mailing list.

Do not return copies of this report unless contractual obligations or notices on a specific document require that it be returned.

REPORT DOCUMENTATION PAGE

Public reporting burden for this collection of information is estimated to average 1 hour per response, including the time for reviewing instructions, searching existing data sources, gathering and maintaining the data needed, and completing and reviewing the collection of information. Send comments regarding this burden estimate or any other aspect of this collection of information, including suggestions for reducing this burden, to Washington Headquarters Services, Directorate for Information Operations and Reports, 1215 Jefferson Davis Highway, Suite 1204, Arlington, VA 22202-4302, and to the Office of Management and Budget, Paperwork Reduction Project (0704-0188), Washington, DC 20503

1. AGENCY USE ONLY (Leave blank)	2. REPORT DATE April 1994	3. REPORT TYPE AND DATES COVERED In-house Sep 92 to Aug 93

4. TITLE AND SUBTITLE
Formulation of Probe-Corrected Time-Domain
Planar Near-Field Measurements

5. FUNDING NUMBERS
PE - 61102F
PR - 2304
TA - 230414
WU - 23041403

6. AUTHOR(S)
Thorkild B. Hansen
Arthur D. Yaghjian

7. PERFORMING ORGANIZATION NAME(S) AND ADDRESS(ES)
Rome Laboratory/ERCT
31 Grenier Street
Hanscom AFB, MA 01731-3010

8. PERFORMING ORGANIZATION REPORT NUMBER

RL-TR--94-74

9. SPONSORING/MONITORING AGENCY NAME(S) AND ADDRESS(ES)

10. SPONSORING/MONITORING AGENCY REPORT NUMBER

11. SUPPLEMENTARY NOTES

Thorkild B. Hansen is a NATO Research Fellow

12a. DISTRIBUTION/AVAILABILITY STATEMENT

Approved for public release; distribution unlimited

12b. DISTRIBUTION CODE

13. ABSTRACT (Maximum 200 words)

Probe-corrected planar near-field formulas in the time domain are derived for both acoustic and electromagnetic fields, so that a single set of near-field measurements in the time domain yields the fields of the test antenna directly in the time domain. The time-domain probe-corrected formulas are first derived by taking the inverse Fourier transform of the corresponding frequency-domain formulas, and then by using a time-domain expansion for the fields of the test antenna and a time-domain receiving characteristic of the probe. Because these general formulas, which involve a double integral over the scan plane and an infinite time-convolution integral, are rather complicated, we consider a special probe whose output due to an incoming time-domain plane wave is proportional to the time derivative of the field of that plane wave. For this special "D-dot probe," the probe-corrected formulas simplify to give the time-domain far-field pattern as a double spatial integral of the time-domain output of the prove over the scan plane multiplied by the angular dependence of the receiving characteristic of the probe. Time-domain reciprocity relations are derived for reciprocal probes, and their time-domain receiving characteristics are related to their far fields. Finally, a time-domain sampling theorem is derived and a numerical

14. SUBJECT TERMS
Near-field measurements   Planar scanning
Time domain   Probe correction

15. NUMBER OF PAGES
42

16. PRICE CODE

17. SECURITY CLASSIFICATION OF REPORT UNCLASSIFIED	18. SECURITY CLASSIFICATION OF THIS PAGE UNCLASSIFIED	19. SECURITY CLASSIFICATION OF ABSTRACT UNCLASSIFIED	20. LIMITATION OF ABSTRACT SAR

example illustrates the use of the time-domain probe-corrected formulas.

Contents

iii

Illustrations

Acknowledgments

Chapter 1

Introduction and Summary of Results

Near-field antenna measurements have been formulated and used extensively during the past three decades to obtain near and far fields of antennas from near-field measurements [1]. In particular, probe-corrected planar near-field measurements were first rigorously formulated in 1963 by Kerns [2], [3] using the plane-wave scattering-matrix theory for antennas and antenna-antenna interactions. Kerns derived the probe-corrected formulas that give the field of an antenna (called the test antenna) everywhere in a half space in terms of near-field data. The near-field data is the output of a probe, with a known receiving characteristic, obtained by scanning on a plane in front of the test antenna. The formulas take into account the receiving characteristic of the probe and assume that multiple interactions between the probe and the test antenna are negligible. All this work was performed in the frequency-domain so that Kerns' formulas determine the fields at one frequency at a time. For antennas excited by short pulses with wide bandwidths it would therefore be convenient to have formulas that determine the time-domain field directly without having to perform the calculations for one frequency at a time.

The purpose of this report is to derive *probe-corrected* planar near-field formulas in the time domain, so that a single set of near-field data in the time domain yields the field of the test antenna directly in the time domain. Formulas are derived for both acoustic and electromagnetic fields and the space outside the region occupied by the test antenna is assumed to be isotropic, homogeneous, and lossless.

The time-domain probe-corrected formulas are derived in two different ways. First, they are derived by taking the inverse Fourier transform of the corresponding frequency-domain formulas. Secondly, they are derived directly in the time domain using a time-domain expansion of the field and a time-domain receiving characteristic of the probe. A previous report [4] derived non-probe-corrected planar near-field formulas in the time domain and numerous results from that report will be used here. For example, the frequency-domain plane-wave spectrum formulas of [4, ch.2] and the time-domain Radon transform formulas of [4, ch.3] will be used extensively.

1

This report is organized as follows. Chapter 2 derives Kerns' frequency-domain, probe-corrected formulas that are relevant for the translation into the time domain. Acoustic fields are treated in Section 2.1 while electromagnetic fields are treated in Section 2.2. (In the electromagnetic case, it proves convenient to define a vector output of the probe.) The derivations are performed by first expanding the field of the test antenna in terms of plane waves [4, ch.2]. Then the definition of the receiving characteristic of the probe and the plane-wave expansion are used to express the output of the probe as a Fourier integral of the receiving characteristic of the probe and the plane-wave spectrum of the test antenna. Finally, the inverse Fourier transform is used to express the plane-wave spectrum of the test antenna in terms of the Fourier transform of the output of the probe and the receiving characteristic of the probe. The special case where the probe is reciprocal is also discussed.

In Chapter 3, we derive the time-domain probe-corrected formulas for both acoustic and electromagnetic fields. In Section 3.1, these formulas are derived for the acoustic field, first by using the inverse Fourier transform and the corresponding frequency-domain formulas of Chapter 2. Then these time-domain probe-corrected formulas are derived directly in the time domain using a time-domain plane-wave expansion of the field radiated by the test antenna and a time-domain receiving characteristic of the probe. These general time-domain probe-corrected formulas involve a double spatial integral (over the scan plane) and a single time-convolution integral (over all times). The integrand in the resulting triple integral is a product of the inverse receiving characteristic of the probe and the output of the probe.

The special case is considered when the output of the probe, due to an incoming time-domain plane wave, is proportional to the time derivative of the plane wave. It is shown that for this type of probe the probe-corrected formulas simplify significantly because it is possible to calculate the time-convolution integral analytically. Specifically, the far-field pattern is given by a double spatial integral (which is simply the Radon transform of the output of the probe) divided by the angular dependence of the receiving characteristic. Finally, reciprocal acoustic probes are considered in Section 3.1. Time-domain reciprocity relations are derived for these probes and their time-domain receiving characteristics are related to their far fields.

In Section 3.2, the time-domain probe-corrected formulas are derived for the electromagnetic field. Also for the electromagnetic field, it is found that the probe-corrected formulas, in general, involve the calculation of a double spatial integral and a time-convolution integral. For probes whose outputs, due to an incoming time-domain plane wave, are proportional to the time derivative of the plane wave, it is found that the time-convolution integral can be calculated analytically. The far field of the test antenna for this type of probe (called a D-dot probe) is given in terms of a double spatial integral only. Finally, in Section 3.2, time-domain reciprocity relations for reciprocal electromagnetic probes are derived.

Section 3.3 outlines two computation schemes to numerically calculate the time-domain far-field patterns from sampled near-field data obtained by using the special type of probe mentioned above. The output of such a probe, due to an incoming time-domain plane wave, is proportional to the time derivative of the field of that plane wave. The two computation schemes are probe-corrected analogs to the non-probe-corrected schemes presented in [4, ch.4].

The first scheme, called the frequency-domain computation scheme, is based on the frequency-domain formulation in Chapter 2. This scheme consists of the following three steps: (1) use the Fourier transform to calculate the frequency-domain output of the probe from the time-domain output, (2) use the frequency-domain probe-corrected formulas of Chapter 2 to calculate the frequency-domain far field from the frequency-domain output of the probe, and (3) use the inverse Fourier transform to calculate the time-domain far field from the frequency-domain far field. This scheme makes use of frequency-domain sampling theorems and the fast Fourier transform (FFT).

The second scheme, called the time-domain computation scheme, is based on the time-domain formulation in Chapter 3. This scheme simply uses the formula that directly gives the time-domain far field in terms of the time-domain output of the probe and its time-domain inverse receiving characteristic. The time-domain sampling theorem from [4, sec.4.2] shows how small the sample spacing between points on the scan plane must be to calculate the far field accurately.

The conclusions of the comparison of two non-probe-corrected computation schemes given in [4, sec.4.4] are also valid for the probe-corrected schemes of this report. Specifically, the direct time-domain computation scheme is much simpler to program and use than the frequency-domain computation scheme. However, because the frequency-domain computation scheme uses the FFT it is much faster for large antennas than the time-domain computation scheme when the full far field is calculated for all times.

When only part of the far field is calculated, the difference in computer time for the two computation schemes becomes smaller and the time-domain computation scheme therefore becomes more advantageous because of its simplicity. Furthermore, the duration of the far-field pattern is extended erroneously because of the finite size of the scan plane, and this longer time-duration has to be taken into account in the frequency-domain calculation scheme. The frequency spacing in the frequency-domain computation scheme has to be chosen small enough so that significant time-domain aliasing is avoided in the calculation of the time-domain far-field pattern. The problem of choosing the frequency spacing small enough does not occur for the time-domain computation scheme because no frequency spacing is used.

Furthermore, the time-domain computation scheme has the capability to calculate the far-field pattern at early times from near-field measurements taken at early times only. This capability is not possessed by the frequency-domain computation scheme because the near field is required for its entire duration to calculate its Fourier transform. For many antennas fed by short pulses, the time dependence of both the near field and far field consists of an early-time part, which contains most of the power, and a late-time part which is oscillatory and contains little power. The duration of the early-time part may be much smaller than the duration of the entire field. If only the early-time part of the far field is of interest, one can use the time-domain computation scheme to determine this part from near-field measurements taken for early times only. Thereby one can significantly reduce the number of near-field time samples needed for the far-field calculation. If instead the frequency-domain computation scheme is used, the number of near-field time samples cannot be reduced because time

samples taken over the entire duration of the near field are needed to calculate the Fourier transform of the near field.

No matter which scheme is chosen, planar time-domain near-field antenna measurements can eliminate the error in the far-field pattern due to the finite scan plane because this error is separated in time from the correct far-field pattern. This makes it possible to use planar scanning in the time domain to compute the far-field of broadbeam antennas in both the time and frequency domains.

Finally, a numerical example illustrates the use of the time-domain computation scheme and one of the acoustic probe-corrected formulas. In this example the far-field pattern of an acoustic point source with Gaussian time dependence is calculated from near-field data obtained by a nonideal probe. The output of this probe, due to an incoming time-domain plane wave, is equal to the time derivative of the plane wave times $\cos\theta$, where θ determines the propagation direction of the plane wave. It is found that the time-domain computation scheme computes the far-field pattern accurately and that the result obtained by neglecting probe correction is very inaccurate for off-axis angles of observation.

Chapter 2

Frequency-Domain Formulas

Probe-corrected planar near-field frequency-domain formulas will be derived in this chapter for both acoustic and electromagnetic fields using a simple, straightforward approach. Those frequency-domain formulas especially useful for the translation of near-field techniques to the time domain will be emphasized. Throughout the report $e^{-i\omega t}$ time dependence is suppressed in all the time-harmonic equations.

2.1 Acoustic Fields

The excess pressure of the acoustic field in a homogeneous isotropic stationary fluid is denoted by Φ, which satisfies the homogeneous Helmholtz equation $\nabla^2\Phi + k^2\Phi = 0$ in every source-free region. Here $k = \omega/c$ is the propagation constant and c is the acoustic speed. In the following the excess pressure Φ is simply called the acoustic field. To use the same terminology as for electromagnetic fields, the acoustic source, which generates the field Φ, will be called the test antenna.

Consider Figure 2.1, showing the geometry for measuring the acoustic field Φ radiated by an acoustic test antenna located in the half space $z < z_0$ and fed by a single propagating mode of amplitude a_0 at the reference plane S_0. Alternatively, one can think of the test antenna as a source region that includes the antenna, the feed system, and the generator, without specifying a waveguide mode with amplitude a_0. This approach was taken in [4].

When the test antenna is the only object in all space it radiates the field given by the plane-wave expansion [3], [4, eqs.(2.8),(2.9)], [5]

$$\Phi(\bar{r}) = \frac{a_0}{2\pi}\int_{-\infty}^{+\infty}\int_{-\infty}^{+\infty} T_0(k_x,k_y)e^{i(k_x x + k_y y + \gamma z)}dk_x dk_y, \quad z \geq z_0 \tag{2.1}$$

where T_0 is the transmitting spectrum of the test antenna given by

$$T_0(k_x,k_y) = \frac{e^{-i\gamma z}}{2\pi a_0}\int_{-\infty}^{+\infty}\int_{-\infty}^{+\infty}\Phi(\bar{r})e^{-i(k_x x + k_y y)}dxdy, \quad z \geq z_0 \tag{2.2}$$

5
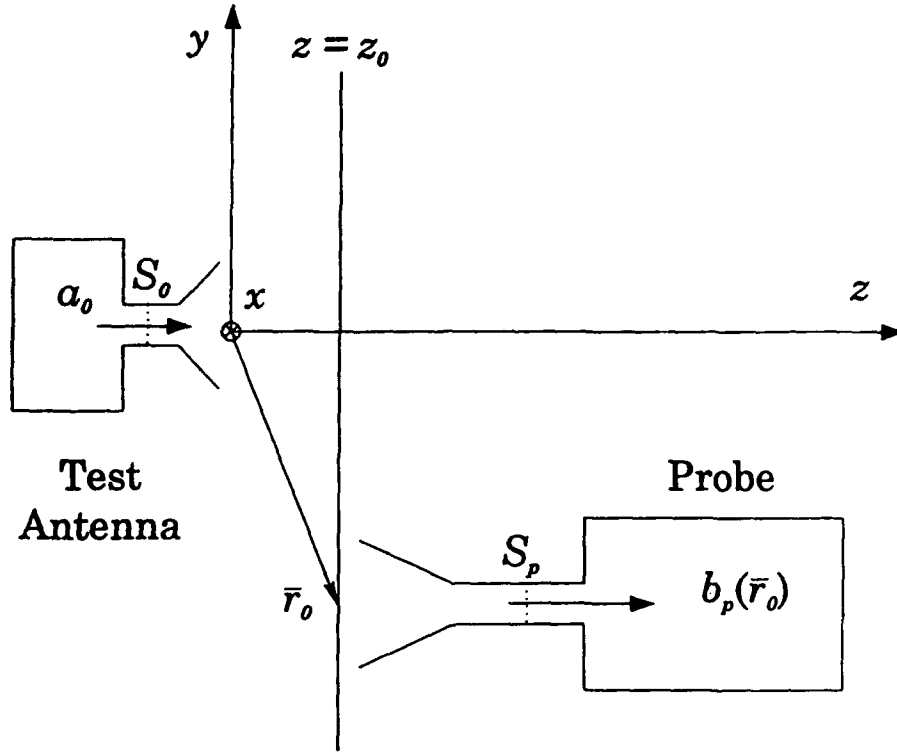
Figure 2.1: Planar scanning geometry.

with

$$\gamma = \begin{cases} |\sqrt{k^2 - k_x^2 - k_y^2}|, & k_x^2 + k_y^2 < k^2 \\ i|\sqrt{k_x^2 + k_y^2 - k^2}|, & k_x^2 + k_y^2 > k^2 \end{cases} \tag{2.3}$$

and $\bar{r} = x\hat{x} + y\hat{y} + z\hat{z}$. The propagation vector for each plane wave can be denoted by $\bar{k} = k_x\hat{x} + k_y\hat{y} + \gamma\hat{z}$. (The product a_0T_0 equals the spectrum T defined in [4].)

The far field of the test antenna, when it is the only object in all space, is given by the well known expression [4, eq.(2.48)]

$$\Phi(\bar{r}) \sim -ia_0k\cos\theta\frac{e^{ikr}}{r}T_0(k\cos\phi\sin\theta, k\sin\phi\sin\theta), \quad z > z_0 \tag{2.4}$$

where the spherical coordinates (r, θ, ϕ) are determined such that $x = r\cos\phi\sin\theta$, $y = r\sin\phi\sin\theta$, and $z = r\cos\theta$. It is convenient to write the far field in terms of the far-field pattern $\mathcal{F}_0(\theta, \phi)$ which is defined such that the far field is $\Phi \sim a_0\mathcal{F}_0(\theta, \phi)e^{ikr}/r$. The far-field expression (2.4) gives the following relation between the spectrum T_0 and the far-field pattern

$$\mathcal{F}_0(\theta, \phi) = -ik\cos\theta T_0(k\cos\phi\sin\theta, k\sin\phi\sin\theta), \quad 0 \le \theta < \pi/2. \tag{2.5}$$

The goal of this section is to calculate the spectrum T_0 for the fixed test antenna by measuring its field on the plane $z = z_0$ using a probe as shown in Figure 2.1. The location

6

of some reference point of the probe is denoted by $\bar{r}_0 = x_0\hat{x} + y_0\hat{y} + z_0\hat{z}$ and in the following the probe is simply said to be located at $\bar{r}_0$ when its reference point is located at $\bar{r}_0$. For planar scanning the probe translates without rotation in the z_0 plane.

Start by assuming that the distance between the probe and the test antenna is always sufficiently large that multiple interactions can be neglected. That is, the reflection in the test antenna, of the field radiated by the induced sources on the probe, does not affect the output of the probe. The effect of the multiple interactions can formally be taken into account by using the plane-wave scattering-matrix theory [3]. However, this theory does not provide quantitative information about these multiple interactions and to obtain useful probe-corrected formulas they have to be neglected. Therefore, we will not use the comprehensive plane-wave scattering-matrix formulation here, but instead use a more direct approach that exhibits the physics of the transmit-receive process. Also, this direct approach can be extended to the time-domain analysis in the next chapter.

The output of the probe at the reference plane S_p is denoted by $b_p(\bar{r}_0)$ and the receiving characteristic of the probe $R_p(k_x, k_y)$ is defined to be the output of the probe, when it is located at $\bar{r}_0 = \bar{0}$ with a fixed orientation in the incident plane wave $(2\pi)^{-1}e^{i(k_x x + k_y y + \gamma z)}$. This means that the output of the probe (when it is located at $\bar{r}_0$) due to the incident plane wave $(2\pi)^{-1}e^{i(k_x x + k_y y + \gamma z)}$ is given by $R_p(k_x, k_y)e^{i(k_x x_0 + k_y y_0 + \gamma z_0)}$. Note that the plane-wave field $(2\pi)^{-1}e^{i(k_x x + k_y y + \gamma z)}$ propagates in the direction given by the spherical angles (θ, ϕ) determined from $k_x = k\cos\phi\sin\theta$ and $k_y = k\sin\phi\sin\theta$ where k is the propagation constant. When $k_x^2 + k_y^2 < k^2$, γ is real and the plane wave is propagating; when $k_x^2 + k_y^2 > k^2$, γ is imaginary and the plane wave is decaying.

Equation (2.1) shows that the plane-wave component of Φ propagating in the direction (k_x, k_y) is given by $a_0(2\pi)^{-1}T_0(k_x, k_y)e^{i(k_x x + k_y y + \gamma z)}dk_x dk_y$ such that the contribution to the output of the probe from this plane-wave component is

$$db_p(\bar{r}_0) = a_0 R_p(k_x, k_y)T_0(k_x, k_y)e^{i(k_x x_0 + k_y y_0 + \gamma z_0)}dk_x dk_y \qquad (2.6)$$

provided multiple interactions between the probe and test antenna are negligible. Also, we are assuming throughout that the probe output line is perfectly matched, so that there is no reflection from its termination. The total output of the probe is thus seen from (2.1) to be the integral over the entire $k_x - k_y$ plane of the expression in (2.6), that is

$$b_p(\bar{r}_0) = a_0 \int_{-\infty}^{+\infty} \int_{-\infty}^{+\infty} R_p(k_x, k_y)T_0(k_x, k_y)e^{i(k_x x_0 + k_y y_0 + \gamma z_0)}dk_x dk_y \qquad (2.7)$$

which is the final expression for the output of the probe located at $\bar{r}_0$. This plane-wave "transmission formula" along with the Fourier transform formulas show directly that the spectrum T_0 for the acoustic field is given by [3], [5]

$$T_0(k_x, k_y) = \frac{e^{-i\gamma z_0}}{(2\pi)^2 a_0 R_p(k_x, k_y)} \int_{-\infty}^{+\infty} \int_{-\infty}^{+\infty} b_p(\bar{r}_0)e^{-i(k_x x_0 + k_y y_0)}dx_0 dy_0. \qquad (2.8)$$

That is, the spectrum T_0 for the acoustic field Φ is simply the Fourier transform of the output of the probe divided by the receiving characteristic R_p of the probe. This is the

general probe-corrected formula which gives the spectrum T_0 for the test antenna in terms of the receiving characteristic and output of the probe.

2.1.1 Formulas for Reciprocal Probes

If the probe is a reciprocal electroacoustic transducer [6], fed by an electromagnetic waveguide in which only a single mode is propagating, the receiving characteristic is given in terms of the spectrum T_p for the probe by the equation [6, eq.(10a)]

$$R_p(k_x, k_y) = \frac{\gamma}{\eta_0 \omega \rho_0} T_p(-k_x, -k_y) \qquad (2.9)$$

where η_0 is the characteristic admittance for the propagating mode in the waveguide feed and ρ_0 is the static pressure of the fluid. Inserting this expression for R_p into the probe-corrected formula (2.8) one finds that the spectrum for the test antenna is given by

$$T_0(k_x, k_y) = \frac{\eta_0 \rho_0 \omega e^{-i\gamma z_0}}{(2\pi)^2 a_0 \gamma T_p(-k_x, -k_y)} \int_{-\infty}^{+\infty} \int_{-\infty}^{+\infty} b_p(\bar{r}_0) e^{-i(k_x x_0 + k_y y_0)} dx_0 dy_0, \qquad (2.10)$$

which is valid when the probe is a reciprocal electroacoustic transducer.

Finally let us express the far-field pattern (2.5) of the test antenna in terms of the far-field pattern of the probe. The far-field pattern of the probe $\mathcal{F}_p(\theta, \phi)$ (with the reference point of the probe at $\bar{r}_0 = 0$ and the spherical angles θ and ϕ measured with respect to the (x, y, z) coordinate system of Figure 2.1) is defined by $\Phi_p \sim a_p \mathcal{F}_p(\theta, \phi) e^{ikr}/r$ where Φ_p is the far field of the probe and a_p is the amplitude of the probe-input signal when the probe is used as a transmit antenna. Since the probe radiates into the half space $z < z_0$, the relation between its far-field pattern $\mathcal{F}_p$ and its spectrum T_p is given by [4, sec.2.2.1], [5, eq.(18)] $\mathcal{F}_p(\theta, \phi) = ik \cos \theta T_p(k \cos \phi \sin \theta, k \sin \phi \sin \theta)$ for $\pi/2 < \theta \leq \pi$. This shows that $T_p(-k \cos \phi \sin \theta, -k \sin \phi \sin \theta) = [ik \cos(\pi - \theta)]^{-1} \mathcal{F}_p(\pi - \theta, \pi + \phi)$, for $0 \leq \theta < \pi/2$ and thus from (2.10) and (2.5) the expression for the far-field pattern of the test antenna is

$$\mathcal{F}_0(\theta, \phi) = -\frac{\eta_0 \rho_0 \omega k \cos \theta}{(2\pi)^2 a_0 \mathcal{F}_p(\pi - \theta, \pi + \phi)} \int_{-\infty}^{+\infty} \int_{-\infty}^{+\infty} b_p(\bar{r}_0) e^{-ik\hat{r} \cdot \bar{r}_0} dx_0 dy_0. \qquad (2.11)$$

Here $\hat{r} = \hat{x} \cos \phi \sin \theta + \hat{y} \sin \phi \sin \theta + \hat{z} \cos \theta$ and $\mathcal{F}_p(\theta, \phi)$ is the far-field pattern of the probe when it is located at $\bar{r}_0 = 0$ of the coordinate system fixed with respect to the test antenna and is radiating alone in the homogeneous fluid (the test antenna is removed). The expression (2.11) gives the far-field pattern of the test antenna as the Fourier transform of the output of the probe divided by the far-field pattern of the probe.

2.2 Electromagnetic Fields

Consider Figure 2.1 showing the geometry for measuring the electric field $\bar{E}$ radiated into free space by the test antenna which is located in the half space $z < z_0$ and is fed by a signal

of amplitude a_0. When the test antenna is the only object in all space it radiates the field $\bar{E}$ given by the plane-wave expansion [3], [4, eqs.(2.10),(2.11)]

$$\bar{E}(\bar{r}) = \frac{a_0}{2\pi} \int_{-\infty}^{+\infty} \int_{-\infty}^{+\infty} \bar{T}_0(k_x, k_y) e^{i(k_x x + k_y y + \gamma z)} dk_x dk_y, \quad z \geq z_0 \tag{2.12}$$

where $\bar{T}_0$ is the transmitting spectrum of the test antenna given by

$$\bar{T}_0(k_x, k_y) = \frac{e^{-i\gamma z}}{2\pi a_0} \int_{-\infty}^{+\infty} \int_{-\infty}^{+\infty} \bar{E}(\bar{r}) e^{-i(k_x x + k_y y)} dx dy, \quad z \geq z_0 \tag{2.13}$$

with $\bar{r} = x\hat{x} + y\hat{y} + z\hat{z}$ and $\bar{k} \cdot \bar{T}_0 = 0$. The far field of the test antenna is given by the well known expression [3], [4, eq.(2.50)]

$$\bar{E}(\bar{r}) \sim -ia_0 k \cos\theta \frac{e^{ikr}}{r} \bar{T}_0(k\cos\phi\sin\theta, k\sin\phi\sin\theta), \quad z > z_0 \tag{2.14}$$

and the far-field pattern

$$\bar{\mathcal{F}}_0(\theta, \phi) = -ik\cos\theta \bar{T}_0(k\cos\phi\sin\theta, k\sin\phi\sin\theta), \quad 0 \leq \theta < \cdot/2. \tag{2.15}$$

for the test antenna is defined such that the far electric field is $\bar{E} \sim a_0 \bar{\mathcal{F}}_0(\theta, \phi) e^{ikr}/r$.

In the following we determine the spectrum $\bar{T}_0$ by measuring the electric field on the plane $z = z_0$ using a probe as shown in Figure 2.1. As for the acoustic field, the probe is located by its reference point $\bar{r}_0$ as measured in the (x, y, z) coordinate system of the test antenna (see Figure 2.1). Again, we assume that the distance between the probe and the test antenna is always large enough for multiple interactions between the test antenna and the probe to be negligible. That is, the reflection in the test antenna, of the field radiated by the induced currents on the probe, does not affect the output of the probe.

The scalar output of the probe is denoted by b_p and it proves convenient to define the vector output of the probe as a vector sum of the scalar output for two mutually perpendicular orientations [7], [8]:

$$\bar{b}_p = b_p^x \hat{x} + b_p^y \hat{y}. \tag{2.16}$$

Here b_p^x and b_p^y are the scalar outputs of the probe when some reference line attached to the probe is parallel to the x and y axis, respectively. For example, if the probe is an open-ended rectangular waveguide the reference line could be chosen such that it is parallel to the longest cross-sectional side of the waveguide.

The dyadic receiving characteristic of the probe $\bar{\bar{R}}_p(k_x, k_y)$ is defined such that the vector output of the probe, when it is located at $\bar{r}_0 = \bar{0}$, due to the incident plane wave $(2\pi)^{-1} \bar{e} e^{i(k_x x + k_y y + \gamma z)}$ with $\bar{e} \cdot \bar{k} = 0$, is given by $\bar{b}_p = \bar{\bar{R}}_p(k_x, k_y) \cdot \bar{e}$. Consequently, the vector output of the probe, when it is located at $\bar{r}_0 = x_0\hat{x} + y_0\hat{y} + z_0\hat{z}$, due to the same incident plane wave, is given by $\bar{b}_p = \bar{\bar{R}}_p(k_x, k_y) \cdot \bar{e} e^{i(k_x x_0 + k_y y_0 + \gamma z_0)}$. The plane-wave expansion (2.12) for the electric field radiated by the test antenna shows that radiated plane-wave component

9

propagating in the direction given by (k_x, k_y) is $a_0(2\pi)^{-1}\bar{T}_0(k_x, k_y)e^{i(k_x x + k_y y + \gamma z)}dk_x dk_y$ and thus the vector output of the probe due to this plane-wave component is

$$d\bar{b}_p(\bar{r}_0) = a_0\overline{\overline{R}}_p(k_x, k_y) \cdot \bar{T}_0(k_x, k_y)e^{i(k_x x_0 + k_y y_0 + \gamma z_0)}dk_x dk_y. \tag{2.17}$$

The total vector output of the probe is thus seen from (2.12) to be the integral over the entire $k_x - k_y$ plane of the expression in (2.17), that is

$$\bar{b}_p(\bar{r}_0) = a_0 \int_{-\infty}^{+\infty} \int_{-\infty}^{+\infty} \overline{\overline{R}}_p(k_x, k_y) \cdot \bar{T}_0(k_x, k_y)e^{i(k_x x_0 + k_y y_0 + \gamma z_0)}dk_x dk_y \tag{2.18}$$

which is the final expression or plane-wave "transmission formula" for the vector out the probe located at $\bar{r}_0$. Taking the inverse Fourier transform of this transmission for   a shows that

$$\overline{\overline{R}}_p(k_x, k_y) \cdot \bar{T}_0(k_x, k_y) = \frac{e^{-i\gamma z_0}}{(2\pi)^2 a_0} \int_{-\infty}^{+\infty} \int_{-\infty}^{+\infty} \bar{b}_p(\bar{r}_0)e^{-i(k_x x_0 + k_y y_0)}dx_0 dy_0 \tag{2.19}$$

from which $\bar{T}_0$ will be determined. Since the vector output of the probe $\bar{b}_p$ is normal to the z axis, (2.19) gives only two equations for determining the three rectangular components of the spectrum $\bar{T}_0$. However, $\bar{T}_0$ satisfies the well-known orthogonality relation [4, eq.(2.12)] $\bar{T}_0(k_x, k_y) \cdot \bar{k} = 0$ so only two equations are necessary for determining $\bar{T}_0$. Because the vector output of the probe (2.16) is perpendicular to $\hat{z}$ the receiving characteristic can be written as

$$\overline{\overline{R}}_p(k_x, k_y) = \hat{x}\bar{R}_p^x(k_x, k_y) + \hat{y}\bar{R}_p^y(k_x, k_y) \tag{2.20}$$

with $\bar{R}_p^x \cdot \bar{k} = 0$ and $\bar{R}_p^y \cdot \bar{k} = 0$. To solve (2.19) for the spectrum $\bar{T}_0$ of the electric field, define the inverse of $\overline{\overline{R}}_p(k_x, k_y)$ by [8]

$$\overline{\overline{R}}_p^{-1}(k_x, k_y) \cdot \overline{\overline{R}}_p(k_x, k_y) = \hat{\theta}(k_x, k_y)\hat{\theta}(k_x, k_y) + \hat{\phi}(k_x, k_y)\hat{\phi}(k_x, k_y) \tag{2.21}$$

where $\hat{\theta}$ and $\hat{\phi}$ are unit vectors orthogonal to $\bar{k}$ satisfying the relations $\hat{\theta} \times \hat{\phi} = \hat{k}$, $\hat{k} \times \hat{\theta} = \hat{\phi}$, and $\hat{\phi} \times \hat{k} = \hat{\theta}$ with $\hat{k}$ defined such that $k\hat{k} = \bar{k} = k_x\hat{x} + k_y\hat{y} + \gamma\hat{z}$. Specifically, $\hat{\theta}$ and $\hat{\phi}$ can be expressed in terms of k_x and k_y as

$$\hat{\theta}(k_x, k_y) = \frac{\gamma k_x}{k\sqrt{k_x^2 + k_y^2}}\hat{x} + \frac{\gamma k_y}{k\sqrt{k_x^2 + k_y^2}}\hat{y} - \frac{\sqrt{k_x^2 + k_y^2}}{k}\hat{z} \tag{2.22}$$

and

$$\hat{\phi}(k_x, k_y) = -\frac{k_y}{\sqrt{k_x^2 + k_y^2}}\hat{x} + \frac{k_x}{\sqrt{k_x^2 + k_y^2}}\hat{y}. \tag{2.23}$$

If $k_x = k\cos\phi\sin\theta$ and $k_y = k\sin\phi\sin\theta$, then $\gamma = k\cos\theta$, and the unit vectors $\hat{\theta}(k_x, k_y)$ and $\hat{\phi}(k_x, k_y)$ are simply the usual angular unit vectors of the spherical coordinate system (k, θ, ϕ) [9, app.1, eqs.(115-116)].

Writing $\overline{\overline{R}}_p^{-1}$ as $\bar{\alpha}\hat{x} + \bar{\beta}\hat{y}$, and assuming that $\hat{k} \cdot \left[\bar{R}_p^y \times \bar{R}_p^x\right] \neq 0$ one finds that the inverse receiving characteristic is given by

$$\overline{\overline{R}}_p^{-1} = \frac{\hat{k} \times \left[\bar{R}_p^y \hat{x} - \bar{R}_p^x \hat{y}\right]}{\hat{k} \cdot \left[\bar{R}_p^y \times \bar{R}_p^x\right]} \tag{2.24}$$

which expresses the inverse receiving characteristic of the probe in terms of the vectors $\bar{R}_p^x = \hat{x} \cdot \overline{\overline{R}}_p$ and $\bar{R}_p^y = \hat{y} \cdot \overline{\overline{R}}_p$. Multiplying (2.19) with $\overline{\overline{R}}_p^{-1}$ and using the definition of the inverse receiving characteristic (2.21) show that the spectrum $\bar{T}_0$ is given by

$$\bar{T}_0(k_x, k_y) = \frac{e^{-i\gamma z_0}}{(2\pi)^2 a_0}\overline{\overline{R}}_p^{-1}(k_x, k_y) \cdot \int_{-\infty}^{+\infty}\int_{-\infty}^{+\infty} \bar{b}_p(\bar{r}_0)e^{-i(k_x x_0 + k_y y_0)}dx_0 dy_0. \tag{2.25}$$

This is the final probe-corrected formula giving the spectrum $\bar{T}_0$ for the electric field radiated into free space by the test antenna as a product of the inverse receiving characteristic of the probe and the Fourier transform of the vector output of the probe.

2.2.1 Formulas for Reciprocal Probes

Now consider the special case of a reciprocal probe that is fed by a waveguide supporting just one propagating mode. Then it follows from [3, ch.2, eq.(1.6-20a)] that the transmitting spectrum of the probe $\bar{T}_p$ is related to the vector receiving characteristic $\bar{R}_p$ by the reciprocity relation

$$\bar{R}_p(k_x, k_y) = \sqrt{\frac{\epsilon}{\mu}}\frac{\gamma}{\eta_0 k}\bar{T}_p(-k_x, -k_y). \tag{2.26}$$

Here ϵ, μ, and η_0 are the permittivity of free space, the permeability of free space, and the characteristic admittance for the propagating mode in the waveguide feed. In Kerns' work [3], $\bar{s}_{20}'$ and $\bar{s}_{02}'$ correspond to our $\bar{T}_p$ and $\bar{R}_p$, and $\bar{s}_{10}$ corresponds to $\bar{T}_0$. The vector receiving characteristic $\bar{R}_p(k_x, k_y)$ of the probe is defined according to [3, ch.2, eqs.(1.3-8),(1.6-14a)] such that the scalar output of the probe (when it is located at $\bar{r}_0 = \bar{0}$), due to the incident plane wave $(2\pi)^{-1}\bar{e}e^{i(k_x x + k_y y + \gamma z)}$ with $\bar{e} \cdot \bar{k} = 0$, is given by $b_p = \bar{R}_p(k_x, k_y) \cdot \bar{e}$. Letting $\bar{T}_p^x$ and $\bar{T}_p^y$ be the transmitting spectra of the probe when it is located at $\bar{r}_0 = \bar{0}$ and its reference line is parallel to the x and y axis, respectively, one sees from (2.20) that $\bar{R}_p^x$ and $\bar{R}_p^y$ are the corresponding vector receiving characteristics of the probe. Applying the reciprocity relation (2.26) to these x and y receiving-transmitting characteristics gives

$$\bar{R}_p^x(k_x, k_y) = \sqrt{\frac{\epsilon}{\mu}}\frac{\gamma}{\eta_0 k}\bar{T}_p^x(-k_x, -k_y), \quad \bar{R}_p^y(k_x, k_y) = \sqrt{\frac{\epsilon}{\mu}}\frac{\gamma}{\eta_0 k}\bar{T}_p^y(-k_x, -k_y). \tag{2.27}$$

One can also see that $\bar{R}_p^x$ and $\bar{R}_p^y$ are vector receiving characteristics corresponding to $\bar{s}_{02}'$ in Kerns' work [3] by comparing the x and y components of the vector transmission formula (2.18) with Kerns' scalar transmission formula [3, ch.2, eq.(3.1-1), and ch.3, eq.(1-12)].

11

Equations (2.27) allow the dyadic receiving characteristic $\overline{\overline{R}}_p$ in (2.20) to be written in terms of the transmitting spectrum of the probe in two different orientations. One may also insert the values of $\bar{R}_p^x(k_x, k_y)$ and $\bar{R}_p^y(k_x, k_y)$ from (2.27) into the expression (2.24) for the inverse of $\overline{\overline{R}}_p$ and then use (2.25) to calculate the transmitting spectrum of the test antenna.

Let us finally express the far-field pattern (2.15) of the test antenna in terms of the vector output of the probe and the far-field patterns, $\bar{\mathcal{F}}_p^x(\theta, \phi)$ and $\bar{\mathcal{F}}_p^y(\theta, \phi)$, of the probe in the two orientations when it is located at $\bar{r}_0 = \bar{0}$. To do this, we use the far-field relation (2.14) and the expression (2.25) for the transmitting spectrum to show that the far-field pattern for the test antenna is given by

$$\bar{\mathcal{F}}_0(\theta, \phi) = -\frac{ik\cos\theta}{(2\pi)^2 a_0} \overline{\overline{R}}_p^{-1}(k\cos\phi\sin\theta, k\sin\phi\sin\theta) \cdot \int_{-\infty}^{+\infty}\int_{-\infty}^{+\infty} \bar{b}_p(\bar{r}_0) e^{-ik\hat{r}\cdot\bar{r}_0} dx_0 dy_0. \quad (2.28)$$

Since the far-field pattern of the probe is to be evaluated in the hemisphere with $z < z_0$ it is found that [3, ch.2, eq.(1.2-16b)], [4, sec.2.2.1] $\bar{\mathcal{F}}_p^x(\theta, \phi) = ik\cos\theta\bar{T}_p^x(k\cos\phi\sin\theta, k\sin\phi\sin\theta)$ for $\pi/2 < \theta \leq \pi$, and the reciprocity relation (2.27) then shows that

$$\bar{R}_p^x(k\cos\phi\sin\theta, k\sin\phi\sin\theta) = \sqrt{\frac{\epsilon}{\mu}}\frac{i}{\eta_0 k}\bar{\mathcal{F}}_p^x(\pi - \theta, \pi + \phi) \quad (2.29)$$

and similarly for $\bar{R}_p^y$. Inserting these results into the expression for the inverse receiving characteristic (2.24) yields

$$\overline{\overline{R}}_p^{-1}(k\cos\phi\sin\theta, k\sin\phi\sin\theta) = \sqrt{\frac{\mu}{\epsilon}}\frac{i\eta_0 k\hat{r} \times \left[\bar{\mathcal{F}}_p^y(\pi - \theta, \pi + \phi)\hat{x} - \bar{\mathcal{F}}_p^x(\pi - \theta, \pi + \phi)\hat{y}\right]}{\hat{r} \cdot \left[\bar{\mathcal{F}}_p^x(\pi - \theta, \pi + \phi) \times \bar{\mathcal{F}}_p^y(\pi - \theta, \pi + \phi)\right]} \quad (2.30)$$

which is the final expression giving the inverse of the dyadic receiving characteristic of the probe in terms of the far-field patterns of the probe in two orientations. Inserting (2.30) into (2.28) gives the far-field pattern of the test antenna in terms of the far-field patterns of the probe and the Fourier transform of the vector output of the probe

$$\bar{\mathcal{F}}_0(\theta, \phi) = \sqrt{\frac{\mu}{\epsilon}}\frac{\eta_0 k^2 \cos\theta}{(2\pi)^2 a_0}\frac{\hat{r} \times \left[\bar{\mathcal{F}}_p^y(\pi - \theta, \pi + \phi)\hat{x} - \bar{\mathcal{F}}_p^x(\pi - \theta, \pi + \phi)\hat{y}\right]}{\hat{r} \cdot \left[\bar{\mathcal{F}}_p^x(\pi - \theta, \pi + \phi) \times \bar{\mathcal{F}}_p^y(\pi - \theta, \pi + \phi)\right]}$$

$$\cdot \int_{-\infty}^{+\infty}\int_{-\infty}^{+\infty} \bar{b}_p(\bar{r}_0) e^{-ik\hat{r}\cdot\bar{r}_0} dx_0 dy_0. \quad (2.31)$$

If the receiving probe is a reciprocal elementary electric dipole, the formula (2.31) for the far field, or more generally, the formula (2.25) for the plane-wave spectrum of the test antenna should reduce to the non-probe-corrected formulas of [4]. To prove this, begin with the expression for the receiving characteristic and output of a reciprocal electric dipole probe [3, p.131]

$$\bar{R}_p^x = \frac{\omega p}{4\pi i a_0 \eta_0}\hat{k} \times \left(\hat{k} \times \hat{x}\right) \quad (2.32)$$

12

$$\bar{R}_p^y = \frac{\omega p}{4\pi i a_0 \eta_0} \hat{k} \times \left(\hat{k} \times \hat{y} \right) \tag{2.33}$$

$$\bar{b}_p = b_p^x \hat{x} + b_p^y \hat{y} = -\frac{\omega p}{2 i a_0 \eta_0} \bar{E}_{xy}(\bar{r}_0) \tag{2.34}$$

where p is the magnitude of the electric dipole moment and $\bar{E}_{xy} = E_x \hat{x} + E_y \hat{y}$ is the transverse electric field of the test antenna in the scan plane. Substituting $\bar{R}_p^x$ and $\bar{R}_p^y$ from (2.32) and (2.33) into (2.24), and simplifying the resulting dyadic expression shows that $\overline{\overline{R}}_p^{-1}$ for the dipole probe can be written as

$$\overline{\overline{R}}_p^{-1} = -\frac{2\pi}{\gamma} \tilde{k} \times (\hat{y}\hat{x} - \hat{x}\hat{y}). \tag{2.35}$$

With $\bar{b}_p$ and $\overline{\overline{R}}_p^{-1}$ from (2.34) and (2.35) inserted into (2.25), the spectrum of the test antenna takes the form

$$\bar{T}(k_x, k_y) = a_0 \bar{T}_0(k_x, k_y) = -\frac{e^{-i\gamma z_0}}{2\pi\gamma} \bar{k} \times \int_{-\infty}^{+\infty} \int_{-\infty}^{+\infty} \hat{z} \times \bar{E}_{xy}(\bar{r}_0) e^{-i(k_x x_0 + k_y y_0)} dx_0 dy_0 \tag{2.36}$$

or

$$\bar{T}(k_x, k_y) = \frac{e^{-i\gamma z_0}}{2\pi} \int_{-\infty}^{+\infty} \int_{-\infty}^{+\infty} \left[\bar{E}_{xy}(\bar{r}_0) - \frac{1}{\gamma} \hat{z} \bar{k} \cdot \bar{E}_{xy}(\bar{r}_0) \right] e^{-i(k_x x_0 + k_y y_0)} dx_0 dy_0. \tag{2.37}$$

Equation (2.37) determines the plane-wave spectrum of the test antenna in terms of the transverse electric field of the test antenna on the scan plane. It is identical to the result obtained for the spectrum of the test antenna from the non-probe-corrected formulas [4, eqs.(2.11)-(2.12)].

In the next chapter, the frequency-domain formulas of this chapter for probe-corrected near-field measurements will be translated into the time domain.

Chapter 3

Time-Domain Formulas

The probe-corrected planar near-field time-domain formulas are derived in this chapter for both acoustic and electromagnetic fields. Section 3.1 derives the formulas for the acoustic field first, by taking the inverse Fourier transform of the corresponding frequency-domain formulas of Section 2.1, and then directly in the time domain. Section 3.2 derives the corresponding formulas for the electromagnetic field. Finally, Section 3.3 uses the probe-corrected formulas to numerically calculate the far-field pattern of an acoustic point source from near-field data obtained by a nonideal probe.

3.1 Acoustic Fields

Without loss of generality we assume that the scan plane is at $z = 0$ because it simplifies the time-domain analysis of this section significantly. Thus, the test antenna is located in the half space $z < 0$ and radiates the time-domain acoustic field $\Phi(\bar{r}, t)$ satisfying the scalar wave equation

$$\nabla^2 \Phi(\bar{r}, t) - \frac{1}{c^2} \frac{\partial^2}{\partial t^2} \Phi(\bar{r}, t) = 0, \quad z > 0 \tag{3.1}$$

where c is the signal speed. The acoustic field $\Phi(\bar{r}, t)$ can be found from its Fourier transform $\Phi_\omega(\bar{r})$ given in Section 2.1, by the Fourier inversion formula

$$\Phi(\bar{r}, t) = \int_{-\infty}^{+\infty} \Phi_\omega(\bar{r}) e^{-i\omega t} d\omega. \tag{3.2}$$

In this chapter all frequency-domain fields are labeled with subscript ω. The time-domain probe-corrected formulas are derived in Subsection 3.1.1 using the Fourier inversion formula (3.2) and the frequency-domain probe-corrected formulas of Section 2.1. Subsection 3.1.3 rederives these formulas by working directly in the time domain with the Radon transform and a time-domain receiving characteristic for the probe. It is shown that the probe-corrected formulas simplify significantly when the probe output due to an incoming plane wave is proportional to the time derivative of the field of that plane wave.

14

Before the time-domain probe-corrected formulas are derived we summarize the time-domain field representation from [4, sec.3.2.2] on which all the time-domain formulas of this report are based. We start by defining the two time-domain functions

$$T_0(\xi, \eta, t) = \int_{-\infty}^{+\infty} T_{0\omega}(\omega\xi, \omega\eta)e^{-i\omega t}d\omega \tag{3.3}$$

and

$$T(\xi, \eta, t) = \int_{-\infty}^{+\infty} a_{0\omega}T_{0\omega}(\omega\xi, \omega\eta)e^{-i\omega t}d\omega = \frac{1}{2\pi}\int_{-\infty}^{+\infty} a_0(t - t')T_0(\xi, \eta, t')dt' \tag{3.4}$$

where $T_{0\omega}$ is the plane-wave spectrum (2.2) of the test antenna, and (ξ, η) are new spectral variables, and $a_{0\omega}$ is the spectrum of the input signal such that $a_0(t) = \int_{-\infty}^{+\infty} a_{0\omega}e^{-i\omega t}d\omega$ is the time dependence of the input signal to the test antenna. Use the definition of T along with the expression (2.2) for the frequency-domain spectrum to get [4, eq.(3.51)]

$$T(\xi, \eta, t) = \frac{1}{2\pi}\int_{-\infty}^{+\infty}\int_{-\infty}^{+\infty} \Phi(\bar{r}_0, t + \xi x_0 + \eta y_0)dx_0 dy_0, \quad \bar{r}_0 = x_0\hat{x} + y_0\hat{y} \tag{3.5}$$

which shows that T is simply the Radon transform of the time-domain field $\Phi(\bar{r}_0, t)$ on the plane $z = 0$ when the test antenna is fed by the input signal $a_0(t)$. The results of [4] show that the time-domain field in the half space $z > 0$ is given by [4, eq.(3.56)]

$$\Phi(\bar{r}, t) = -\frac{1}{2\pi}\int\int_{\xi^2+\eta^2<c^{-2}} \frac{\partial^2}{\partial t^2}T(\xi, \eta, t - \xi x - \eta y - \zeta z)d\xi d\eta$$

$$-\frac{1}{2\pi^2}\int\int_{\xi^2+\eta^2>c^{-2}}\int_{-\infty}^{+\infty} \frac{|\zeta|z}{|\zeta|^2z^2 + t'^2}\frac{\partial^2}{\partial t^2}T(\xi, \eta, t - t' - \xi x - \eta y)dt'd\xi d\eta, \quad z > 0 \tag{3.6}$$

where

$$\zeta = \begin{cases} |\sqrt{c^{-2} - \xi^2 - \eta^2}|, & \xi^2 + \eta^2 < c^{-2} \\ i|\sqrt{\xi^2 + \eta^2 - c^{-2}}|, & \xi^2 + \eta^2 > c^{-2} \end{cases} \tag{3.7}$$

Furthermore, the time-domain far field is given by the simple expression [4, eq.(3.59)]

$$\Phi(\bar{r}, t) \sim \frac{\cos\theta}{cr}\frac{\partial}{\partial t}T(c^{-1}\cos\phi\sin\theta, c^{-1}\sin\phi\sin\theta, t - r/c), \quad 0 \leq \theta < \pi/2. \tag{3.8}$$

These expressions show that the field radiated by the test antenna into the half space $z > 0$ is completely determined from the Radon transform $T(\xi, \eta, t)$ of the field on the plane $z = 0$. Writing the time-domain far-field as $\Phi(\bar{r}, t) \sim \mathcal{F}(\theta, \phi, t - r/c)/r$, where $\mathcal{F}$ is the time-domain far-field pattern, we find from (3.8) that

$$\mathcal{F}(\theta, \phi, t) = \frac{\cos\theta}{c}\frac{\partial}{\partial t}T(c^{-1}\cos\phi\sin\theta, c^{-1}\sin\phi\sin\theta, t), \quad 0 \leq \theta < \pi/2. \tag{3.9}$$

The formulas (3.5)-(3.9) constitute the time-domain field representation that gives the field in the half space $z > 0$ in terms of the Radon transform of the field on the plane $z = 0$.

Having summarized the time-domain field representations, we will now derive expressions that give the Radon transform T or the far-field pattern $\mathcal{F}$ in terms of the output and receiving characteristic of the probe.

15

3.1.1 Formulas Obtained from the Fourier Transform

We begin by deriving the time-domain probe-corrected formulas using the Fourier transform along with the frequency-domain formulas of Section 2.1. The frequency-domain probe-corrected formula (2.8) shows that with $\bar{r}_0 = x_0\hat{x} + y_0\hat{y}$

$$T_\omega(\omega\xi, \omega\eta) = a_{0\omega}T_{0\omega}(\omega\xi, \omega\eta) = \frac{1}{(2\pi)^2 R_{p\omega}(\omega\xi, \omega\eta)} \int_{-\infty}^{+\infty}\int_{-\infty}^{+\infty} b_{p\omega}(\bar{r}_0)e^{-i\omega(\xi x_0 + \eta y_0)}dx_0dy_0 \tag{3.10}$$

where $R_{p\omega}$ and $b_{p\omega}$ are the frequency-domain receiving characteristic and output, respectively, of the probe. Introduce the inverse time-domain receiving characteristic of the probe defined by [1]

$$R_p^{-1}(\xi, \eta, t) = \int_{-\infty}^{+\infty} \frac{e^{-i\omega t}}{R_{p\omega}(\omega\xi, \omega\eta)}d\omega. \tag{3.11}$$

Use the convolution rule

$$\int_{-\infty}^{+\infty} f_\omega g_\omega e^{-i\omega t}d\omega = \frac{1}{2\pi}\int_{-\infty}^{+\infty} f(t')g(t - t')dt' \tag{3.12}$$

in taking the inverse Fourier transform of (3.10) to get the following three alternative formulas for the Radon transform T

$$T(\xi, \eta, t) = \frac{1}{(2\pi)^3}\int_{-\infty}^{+\infty} R_p^{-1}(\xi, \eta, t')\int_{-\infty}^{+\infty}\int_{-\infty}^{+\infty} b_p(\bar{r}_0, t - t' + \xi x_0 + \eta y_0)dx_0dy_0dt' \tag{3.13}$$

$$T(\xi, \eta, t) = \frac{1}{(2\pi)^3}\int_{-\infty}^{+\infty}\int_{-\infty}^{+\infty}\int_{-\infty}^{+\infty} R_p^{-1}(\xi, \eta, t - t' + \xi x_0 + \eta y_0)b_p(\bar{r}_0, t')dx_0dy_0dt' \tag{3.14}$$

and

$$T(\xi, \eta, t) = \frac{1}{(2\pi)^3}\int_{-\infty}^{+\infty}\int_{-\infty}^{+\infty}\int_{-\infty}^{+\infty} R_p^{-1}(\xi, \eta, t - t' + \xi x_0 + \eta y_0)b_p(\bar{r}_0, t')dt'dx_0dy_0 \tag{3.15}$$

where $\bar{r}_0 = x_0\hat{x} + y_0\hat{y}$ and $b_p(\bar{r}_0, t')$ is the time-domain output of the probe when it is located at $\bar{r}_0$. The formulas (3.13), (3.14), and (3.15) are the general time-domain probe-corrected formulas giving the Radon transform of the field in terms of the output and receiving characteristic of the probe.

Assume that the test antenna is turned on at $t = t_0$ so that all fields are zero for $t < t_0$. Then the output of the probe $b_p(\bar{r}_0, t)$ is zero for $\bar{r}_0 \notin \rho(t)$ where $\rho(t)$ is the finite region of the scan plane on which the field is nonzero at time t. (For late times, $\rho(t)$ is approximately a circular disk with radius $c(t - t_0)$.) Without making any assumption about the time dependence of the inverse receiving characteristic R_p^{-1}, the probe-corrected formulas all involve at least one integral over an infinite region. For example, the (x_0, y_0) integral in

---

[1] Both the time-domain receiving characteristic $R_p(\xi, \eta, t) = \int_{-\infty}^{+\infty} R_{p\omega}(\omega\xi, \omega\eta)e^{-i\omega t}d\omega$ and its inverse defined by (3.11) can be generalized functions. This will be seen from Section 3.1.3 where these functions are defined directly in the time domain.

(3.14) becomes an integral over the finite region $\rho(t')$, but the t' integration goes from $t' = t_0$ to $t' = +\infty$ and thus involves an integration over an infinite region. Similar statements hold for the probe-corrected formulas (3.13) and (3.15). However, as we shall see later in this section, only integrals over finite regions need be calculated to get the time-domain far-field pattern when a special type of probe is used.

Equation (3.15) may be the most attractive for measurement purposes since the inner time integral can be calculated at each scan point $\bar{r}_0$ for the desired values of (ξ, η, t). Thus one would not have to store the values of the output of the probe $b_p(\bar{r}_0, t')$ over time to calculate the Radon transform of the field radiated by the test antenna.

Having determined the Radon transform $T(\xi, \eta, t)$ one can then use (3.6) to calculate the time-domain field everywhere in the half space $z > 0$ or use (3.9) to calculate the time-domain far-field pattern. Note also that instead of the real time-domain Radon transform formulas (3.5)-(3.8) one could have used the complex formulas of [4, sec.3.2.3] involving the analytic fields. The expressions for the field in the half space $z > 0$ would then have been given by the simpler expression [4, eq.(3.78)], which however involves the analytic fields that cannot be measured directly. Thus, for measurement purposes, the real Radon transform formulas used in this report seem advantageous compared to the complex Radon transform formulas. This was discussed more fully in the previous report [4].

3.1.2 Formulas for Time-Derivative Probes

The general time-domain probe-corrected formulas (3.13)-(3.15) require the calculation of a triple integral involving an infinite time integral. We will now show that for a special type of probe, which has been used for time-domain electromagnetic measurements [10], [11], the infinite time integral can be evaluated analytically. The outputs of these probes due to incoming plane waves are proportional to the time derivative of the field in the incoming wave, that is, the frequency-domain receiving characteristic is proportional to ω and can be written as

$$R_{p\omega}(\omega\xi, \omega\eta) = -\frac{i\omega Q_p(\xi, \eta)}{2\pi} \tag{3.16}$$

where the angularly dependent function $Q_p(\xi, \eta)$ is independent of the frequency. With the receiving characteristic (3.16) inserted into the probe-corrected formula (3.10), the inverse Fourier transform of (3.10) gives

$$\frac{\partial}{\partial t} T(\xi, \eta, t) = \frac{1}{2\pi Q_p(\xi, \eta)} \int_{-\infty}^{+\infty} \int_{-\infty}^{+\infty} b_p(\bar{r}_0, t + \xi x_0 + \eta y_0) dx_0 dy_0 \tag{3.17}$$

which expresses the time derivative of the Radon transform of the near field as the Radon transform of the output of the probe divided by the angularly dependent function Q_p. The far-field expression (3.9) shows that the time-domain far-field pattern is given by

$$\mathcal{F}(\theta, \phi, t) = \frac{\cos\theta \int_{-\infty}^{+\infty} \int_{-\infty}^{+\infty} b_p(\bar{r}_0, t + \hat{r} \cdot \bar{r}_0/c) dx_0 dy_0}{2\pi c Q_p(c^{-1}\cos\phi\sin\theta, c^{-1}\sin\phi\sin\theta)}. \tag{3.18}$$

17

Thus, when the probe has the simple receiving characteristic (3.16), the far field of the test antenna is simply the Radon transform of the output of the probe divided by the angular dependence of the probe receiving characteristic.

Let us again assume that the test antenna is turned on at $t = t_0$ so that the output of the probe $b_p(\bar{r}_0, t)$ is zero when $\bar{r}_0$ is outside the region $\rho(t)$. Then the integrand of (3.17) is zero when $\bar{r}_0$ is outside the region $\rho(t + \xi x_0 + \eta y_0)$. For late times, when the finite region $\rho(t)$ is approximately a circle of radius $c(t - t_0)$, this translates into: $b_p(\bar{r}_0, t) = 0$ for $|\bar{r}_0| > c(t - t_0) + c\xi x_0 + c\eta y_0$. When $\xi^2 + \eta^2 > c^{-2}$ this condition is not satisfied no matter how large $|\bar{r}_0|$ may be, so in this situation the region of integration in (3.17) is infinite. When $\xi^2 + \eta^2 < c^{-2}$ this condition is satisfied for all $|\bar{r}_0|$ larger than some finite number and the region of integration in (3.17) (and (3.18)) is finite. Consequently, when the time-domain far-field pattern is calculated with a probe whose receiving characteristic satisfies (3.16), the integral is over a finite region. Thus, the far-field pattern can be calculated at early times from measured data taken on a finite scan plane without introducing any error caused by the finite scan plane. This property of the special time-domain probe-corrected formula (3.18) is not possessed by any of the frequency-domain probe-corrected formulas and, as discussed in [4, ch.4], makes it possible to use planar time-domain scanning for broadbeam antennas.

3.1.3 Formulas Obtained Directly in the Time Domain

This subsection derives the probe-corrected acoustic formulas directly in the time domain using the Radon transform and a time-domain receiving characteristic for the probe. To define a time-domain receiving characteristic of the probe, one has to specify the time-domain basis fields that will be used to expand the field radiated by the test antenna. We choose the time-domain basis fields to be simply the inverse Fourier transform of the propagating and decaying plane waves used to expand the frequency-domain fields. To facilitate the time-domain analysis, the spectral variables (k_x, k_y) are replaced by (ξ, η) defined by $(k_x, k_y) = (\omega\xi, \omega\eta)$ for all real ω and we only consider fields in the half space $z > 0$. Furthermore, we write the frequency-domain plane wave $(2\pi)^{-1} e^{i(k_x x + k_y y + \gamma z)}$ as

$$\Phi_\omega^B(\bar{r}, \xi, \eta) = \frac{1}{2\pi} \begin{cases} e^{i\omega(\xi x + \eta y + \zeta z)}, & \omega > 0 \\ e^{i\omega(\xi x + \eta y + \zeta^* z)}, & \omega < 0 \end{cases} \tag{3.19}$$

where $-\infty < \xi < +\infty$, $-\infty < \eta < +\infty$, $z > 0$, and $*$ denotes complex conjugation. Taking the inverse Fourier transform (3.2) of equation (3.19) shows that the time-domain basis fields are

$$\Phi^B(\bar{r}, t, \xi, \eta) = \begin{cases} \delta(t - \xi x - \eta y - \zeta z), & \xi^2 + \eta^2 < c^{-2} \\ \frac{\pi^{-1} z |\zeta|}{z^2 |\zeta|^2 + (t - \xi x - \eta y)^2}, & \xi^2 + \eta^2 > c^{-2} \end{cases} \tag{3.20}$$

where $z > 0$ and the identity

$$\int_{-\infty}^{+\infty} e^{-|\omega||\zeta|z} e^{-i\omega t} d\omega = \frac{2|\zeta| z}{|\zeta|^2 z^2 + t^2}, \quad z > 0 \tag{3.21}$$
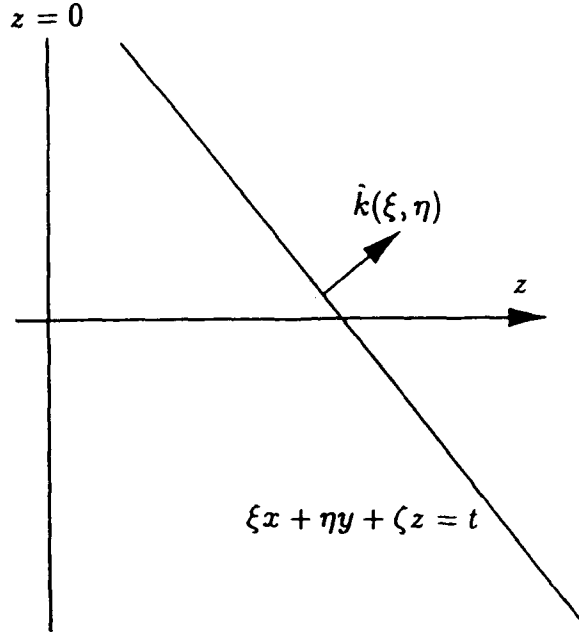
18

Figure 3.1: Propagating time-domain plane wave.

has been used.

Since these time-domain basis fields are obtained from frequency-domain plane waves, we will refer to them as time-domain plane waves. As will be seen below, the time-domain plane waves $\Phi^B(\bar{r}, t, \xi, \eta)$ constitute a complete set of functions for expanding the time-domain field radiated by the test antenna.

Let us study the physical properties of these time-domain plane waves. The propagating plane wave $\Phi^B(\bar{r}, t, \xi, \eta)$, $\xi^2 + \eta^2 < c^{-2}$ is a delta function which is nonzero only on the plane $t = \xi x + \eta y + \zeta z$ and is propagating in the direction given by the unit vector $\hat{k}(\xi, \eta) = c\xi\hat{x} + c\eta\hat{y} + c\zeta\hat{z}$ as shown in Figure 3.1. The decaying plane wave $\Phi^B(\bar{r}, t, \xi, \eta)$, $\xi^2 + \eta^2 > c^{-2}$ is more complicated. On the plane $\xi x + \eta y = t_0$, which is parallel to the z axis, the amplitude of the decaying plane wave has a maximum at $z = |t - t_0|/|\zeta|$ and decays as z^{-1} at infinity as shown in Figure 3.2. Furthermore, from the analysis of Morse and Feshbach [13, pp.813-814] it follows that

$$\lim_{z|\zeta|\to 0_+} \frac{\pi^{-1} z|\zeta|}{z^2|\zeta|^2 + (t - \xi x - \eta y)^2} = \delta(t - \xi x - \eta y) \tag{3.22}$$

so that, in agreement with (3.19), all time-domain plane waves are delta functions on the plane $z = 0$.

Having defined and studied the time-domain plane waves, let us now turn to the time-domain receiving characteristic of the probe. This characteristic is denoted by $R_p(\xi, \eta, t)$ and is defined to be the output of the probe, when its reference point is located at $\bar{r}_0 = 0$, and the incoming wave is the plane wave $\Phi^B(\bar{r}, t, \xi, \eta)$ given in (3.20). From the expression (3.20) for
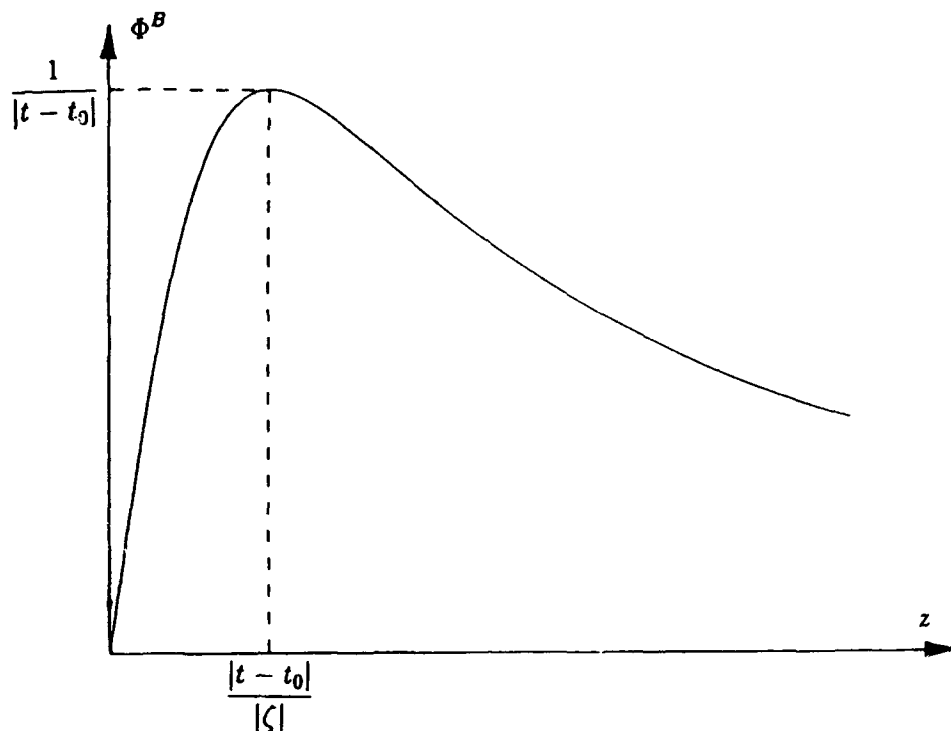
19

Figure 3.2: Decaying time-domain plane wave on the plane $\xi x + \eta y = t_0$.

the plane wave it is seen that the output of the probe, when it is located at $\bar{r}_0 = x_0\hat{x} + y_0\hat{y}$, is given by $R_p(\xi, \eta, t - \xi x_0 - \eta y_0)$ as illustrated in Figure 3.3.

Now that both the time-domain plane waves and the time-domain receiving characteristic of the probe have been defined, v. can calculate the output of the probe due to the field radiated by the test antenna. To do this note that the expression (3.6) for the field radiated by the test antenna can be written in terms of the time-domain plane waves as the time-convolution integral

$$\Phi(\bar{r}, t) = -\frac{1}{2\pi} \int_{-\infty}^{+\infty} \int_{-\infty}^{+\infty} \int_{-\infty}^{+\infty} \Phi^B(\bar{r}, t - t', \xi, \eta) \frac{\partial^2}{\partial t'^2} T(\xi, \eta, t') dt' d\xi d\eta, \quad z > 0. \qquad (3.23)$$

This expression enables us to derive the expression for the output of the probe $b_p(\bar{r}_0, t)$ when it is located at $\bar{r}_0$ and the incident field is that of the test antenna. We assume that the distance between the probe and the test antenna is large enough that multiple interactions between the test antenna and the probe can be neglected. That is, the reflection in the test antenna, of the field radiated by the induced currents on the probe, does not affect the output of the probe.

The output of the probe from the component $-(2\pi)^{-1}\Phi^B(\bar{r}, t - t', \xi, \eta)\frac{\partial^2}{\partial t'^2}T(\xi, \eta, t')dt'd\xi d\eta$ of the incident field is, according to the definition of the probe receiving characteristic, given by

$$db_p(\bar{r}_0, t) = -\frac{1}{2\pi} R_p(\xi, \eta, t - t' - \xi x_0 - \eta y_0)\frac{\partial^2}{\partial t'^2}T(\xi, \eta, t')dt'd\xi d\eta \qquad (3.24)$$
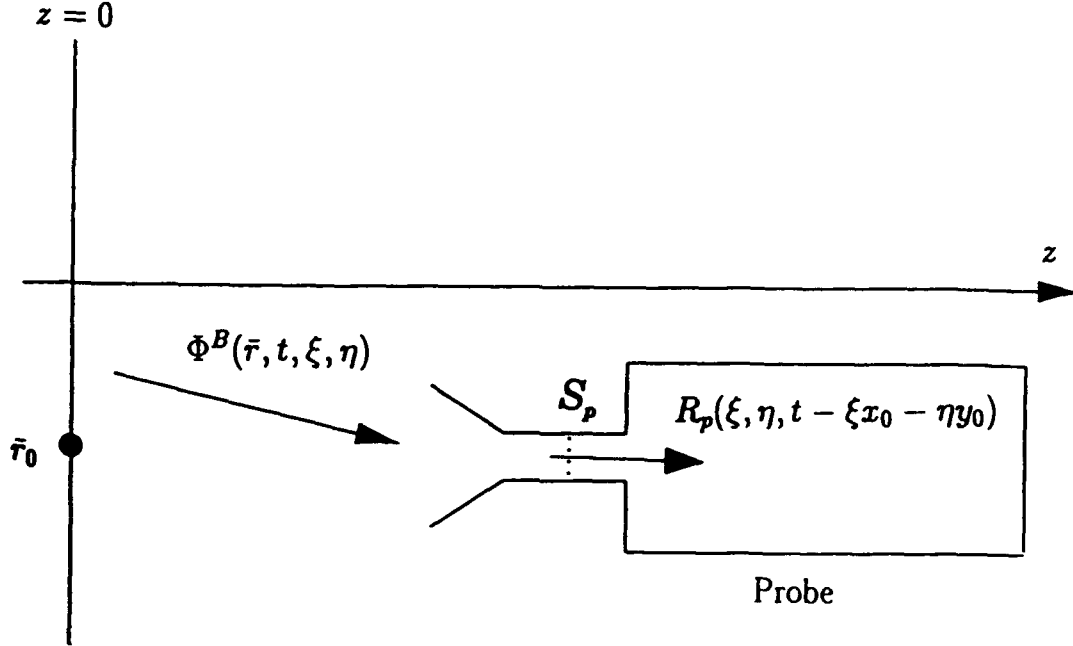
20

Figure 3.3: Output of probe due to the incoming plane wave $\Phi^B(\bar{r}, t, \xi, \eta)$. The reference point of the probe is located at $\bar{r}_0 = x_0\hat{x} + y_0\hat{y}$.

and the total output of the probe is thus seen from (3.23) to be

$$b_p(\bar{r}_0, t) = -\frac{1}{2\pi} \int_{-\infty}^{+\infty} \int_{-\infty}^{+\infty} \int_{-\infty}^{+\infty} R_p(\xi, \eta, t - t' - \xi x_0 - \eta y_0) \frac{\partial^2}{\partial t'^2} T(\xi, \eta, t') dt' d\xi d\eta. \quad (3.25)$$

To determine the Radon transform $T(\xi, \eta, t')$ from this equation, define the inverse time-domain receiving characteristic $R_p^{-1}(\xi, \eta, t)$ for the probe in accordance with (3.11) by

$$\int_{-\infty}^{+\infty} R_p^{-1}(\xi, \eta, t') R_p(\xi, \eta, t - t') dt' = 4\pi^2 \delta(t), \quad (3.26)$$

multiply the expression (3.25) for the total output of the probe by $R_p^{-1}(\xi, \eta, t'' - t)$, and integrate it with respect to t to get

$$\int_{-\infty}^{+\infty} b_p(\bar{r}_0, t) R_p^{-1}(\xi, \eta, t'' - t) dt = -2\pi \int_{-\infty}^{+\infty} \int_{-\infty}^{+\infty} \frac{\partial^2}{\partial t''^2} T(\xi, \eta, t'' - \xi x_0 - \eta y_0) d\xi d\eta. \quad (3.27)$$

The Radon transform pairs (3.5) and (3.6) (see also [12, p.111])

$$T(\xi, \eta, t) = \frac{1}{2\pi} \int_{-\infty}^{+\infty} \int_{-\infty}^{+\infty} \Phi(\bar{r}_0, t + \xi x_0 + \eta y_0) dx_0 dy_0 \quad (3.28)$$

$$\Phi(\bar{r}_0, t) = -\frac{1}{2\pi} \int_{-\infty}^{+\infty} \int_{-\infty}^{+\infty} \frac{\partial^2}{\partial t^2} T(\xi, \eta, t - \xi x_0 - \eta y_0) d\xi d\eta \quad (3.29)$$

21

with $\bar{r}_0 = x_0\hat{x} + y_0\hat{y}$, along with (3.27), now show that the Radon transform of the field radiated by the test antenna on the plane $z = 0$ is given by

$$T(\xi,\eta,t) = \frac{1}{(2\pi)^3} \int_{-\infty}^{+\infty} \int_{-\infty}^{+\infty} \int_{-\infty}^{+\infty} R_p^{-1}(\xi,\eta,t - t' + \xi x_0 + \eta y_0) b_p(\bar{r}_0, t') dt' dx_0 dy_0. \quad (3.30)$$

This expression is seen to agree with the result (3.15) found by Fourier transforming the corresponding frequency-domain result. Equation (3.30) is the time-domain probe-corrected formula derived directly in the time domain using the Radon transform and a time-domain expansion of the field radiated by the test antenna. Interchanging the orders of integration in (3.30) produces the probe-corrected formulas (3.13) and (3.14).

Formulas for time-derivative probes

Let us again turn to the special case where the output of the probe due to an incoming plane wave is proportional to the time derivative of the plane wave. In this case the time-domain receiving characteristic takes the form

$$R_p(\xi,\eta,t) = Q_p(\xi,\eta)\frac{\partial}{\partial t}\Phi^B(\bar{0},t,\xi,\eta) = Q_p(\xi,\eta)\delta'(t) \quad (3.31)$$

which is valid for all (ξ,η) and is in accordance with the frequency-domain result (3.16). The last part of (3.31) is obtained by using the expressions (3.20) and (3.22) to get the values of the plane waves on the plane $z = 0$. The definition (3.26) for the time-domain inverse receiving characteristic and the expression (3.31) for the receiving characteristic show that

$$\frac{\partial}{\partial t}R_p^{-1}(\xi,\eta,t) = \frac{(2\pi)^2\delta(t)}{Q_p(\xi,\eta)} \quad (3.32)$$

for all (ξ,η). Taking the time derivative of the probe-corrected formula (3.30) and inserting this value for the time derivative of R_p^{-1}, one recovers the probe-corrected formula (3.17) derived from the corresponding frequency-domain result. It has now been demonstrated once more that the probe-corrected formulas simplify considerably when the output of the probe due to an incoming plane wave is proportional to the time derivative of the plane wave.

3.1.4 Formulas for Reciprocal Probes

In the previous two subsections the probe-corrected formulas were derived for arbitrary probes and for probes whose output is proportional to the time derivative of an incoming plane wave. This subsection derives probe-corrected formulas for cases where the probe is a reciprocal electroacoustic transducer [6]. It is shown that there is a simple relation between the time-domain receiving characteristic $R_p(\xi,\eta,t)$ and the time-domain transmitting characteristic $T_p^\delta(\xi,\eta,t)$ of the probe. Here $T_p^\delta(\xi,\eta,t)$ is simply the Radon transform (3.5) of the field radiated by the probe into the half space $z < 0$ when it is located at $\bar{r}_0 = 0$ and is fed by the delta-function input signal $a_p(t) = 2\pi\delta(t)$, as shown in Figure 3.4.
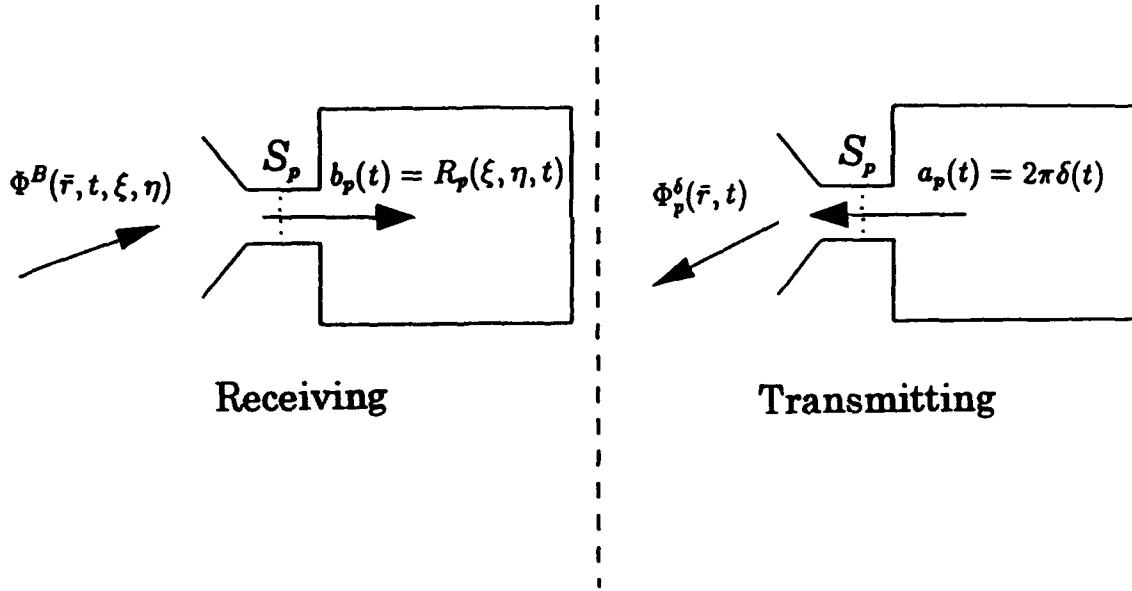
22

$$\Phi^B(\bar{r}, t, \xi, \eta) \qquad S_p \qquad b_p(t) = R_p(\xi, \eta, t) \qquad \Phi^\delta_p(\bar{r}, t) \qquad S_p \qquad a_p(t) = 2\pi\delta(t)$$

Receiving   Transmitting

Figure 3.4: Geometry for reciprocity relations.

The field radiated by the probe into the half space $z < 0$ in this situation is denoted by Φ^δ_p and is given by the time-convolution integral (3.23) with T replaced by T^δ_p, and with Φ^B being the time-domain plane waves for the half space $z < 0$ given by (3.20) with z replaced by $-z$. The delta-function far-field of the probe is given by the negative of (3.8), that is

$$\Phi^\delta_p(\bar{r}, t) \sim -\frac{\cos\theta}{cr}\frac{\partial}{\partial t}T^\delta_p(c^{-1}\cos\phi\sin\theta, c^{-1}\sin\phi\sin\theta, t - r/c), \quad \pi/2 < \theta \le \pi \qquad (3.33)$$

and the corresponding far-field pattern is

$$\mathcal{F}^\delta_p(\theta, \phi, t) = -\frac{\cos\theta}{c}\frac{\partial}{\partial t}T^\delta_p(c^{-1}\cos\phi\sin\theta, c^{-1}\sin\phi\sin\theta, t), \quad \pi/2 < \theta \le \pi \qquad (3.34)$$

where $\mathcal{F}^\delta_p$ is defined such that the delta-function far-field is $\Phi^\delta_p(\bar{r}, t) \sim \mathcal{F}^\delta_p(\theta, \phi, t - r/c)/r$.

Assume now that the probe is a reciprocal electroacoustic transducer [6]. Then from (2.9) the following frequency-domain reciprocity relation exists for all real ω between its frequency-domain receiving and transmitting characteristics

$$R_{p\omega}(\xi\omega, \eta\omega) = \begin{cases} \frac{\zeta}{\eta_0\rho_0}T^\delta_{p\omega}(-\xi\omega, -\eta\omega), & \xi^2 + \eta^2 < c^{-2} \\ \frac{\omega}{|\omega|}\frac{\zeta}{\eta_0\rho_0}T^\delta_{p\omega}(-\xi\omega, -\eta\omega), & \xi^2 + \eta^2 > c^{-2} \end{cases} \qquad (3.35)$$

where the fact that any frequency-domain function must satisfy $f_\omega = f^*_{-\omega}$ has been used. Taking the inverse Fourier transform of (3.35) and using the fact that the real and imaginary

parts of an analytic function on the real axis are related through the Hilbert transform [13, pp.370-372] reveal the following time-domain reciprocity relation

$$R_p(\xi, \eta, t) = \begin{cases} \frac{\zeta}{\eta_0 \rho_0} T_p^\delta(-\xi, -\eta, t), & \xi^2 + \eta^2 < c^{-2} \\ \frac{|\zeta|}{\eta_0 \rho_0} \mathcal{H} T_p^\delta(-\xi, -\eta, t), & \xi^2 + \eta^2 > c^{-2} \end{cases} \quad (3.36)$$

where $\mathcal{H}$ denotes the Hilbert transform given by

$$\mathcal{H}f(t) = \fint_{-\infty}^{+\infty} \frac{f(t')}{\pi(t - t')} dt'. \quad (3.37)$$

The bar on the integral sign indicates a Cauchy principal value integration (see [4, sec.3.2.3]). Note that the time-domain reciprocity relation (3.36) is simple and similar to the corresponding frequency-domain relation (2.9) as long as $\xi^2 + \eta^2 < c^{-2}$ (propagating plane waves); however it is more complicated and involves the Hilbert transform when $\xi^2 + \eta^2 > c^{-2}$ (decaying plane waves).

The time-domain reciprocity relation (3.36) with $\zeta = -c^{-1} \cos\theta$ now gives the following relation between the delta-function far-field pattern $\mathcal{F}_p^\delta$ (3.34) and the receiving characteristic of the probe

$$\mathcal{F}_p^\delta(\theta, \phi, t) = \eta_0 \rho_0 \frac{\partial}{\partial t} R_p(c^{-1} \cos(\pi + \phi) \sin(\pi - \theta), c^{-1} \sin(\pi + \phi) \sin(\pi - \theta), t), \quad \pi/2 < \theta \le \pi. \quad (3.38)$$

Consequently, for reciprocal probes, the delta-function far-field pattern is proportional to the time derivative of the time-domain receiving characteristic. Since the delta-function far-field pattern is equal to the time derivative of the step-function far-field pattern, it is seen that the step-function far-field pattern of a reciprocal probe is proportional to its time-domain receiving characteristic.

Finally assume that the probe receiving characteristic satisfies (3.31) in addition to the reciprocity relation (3.36), that is, the output of the probe from an incoming plane wave is proportional to the time derivative of the plane-wave field. Then (3.31) combines with (3.38) to produce

$$\mathcal{F}_p^\delta(\theta, \phi, t) = \eta_0 \rho_0 Q_p(c^{-1} \cos(\pi + \phi) \sin(\pi - \theta), c^{-1} \sin(\pi + \phi) \sin(\pi - \theta)) \delta''(t), \quad \pi/2 < \theta \le \pi \quad (3.39)$$

which shows that the angular dependence of the delta-function far-field is that of the receiving characteristic and the time dependence of the far-field pattern is the second derivative of a delta function. Consequently, the far-field of this particular reciprocal probe is related to the second time derivative of the signal feeding the probe.

3.2 Electromagnetic Fields

This section derives the probe-corrected formulas for the electromagnetic fields. The derivations are very similar to the ones for the acoustic field since each of the rectangular components of the electric field satisfies the acoustic-field formulas. Therefore, nearly all of the

formulas for the electromagnetic fields can be obtained easily by modifying the corresponding formulas for the acoustic field.

First we summarize the Radon transform formulas for the electric field, which allow us to calculate the electric field everywhere in the half space $z > 0$ in terms of the field on the plane $z = 0$. We assume that the test antenna is fed by the time signal $a_0(t)$ and introduce the Radon transform of the electric field on the plane $z = 0$ by [4, eq.(3.61)]

$$\bar{T}(\xi, \eta, t) = \frac{1}{2\pi} \int_{-\infty}^{+\infty} \int_{-\infty}^{+\infty} \bar{E}(\bar{r}_0, t + \xi x_0 + \eta y_0) dx_0 dy_0, \quad \bar{r}_0 = x_0 \hat{x} + y_0 \hat{y}. \tag{3.40}$$

Because $\nabla \cdot \bar{E} = 0$ the Radon transform of the electric field satisfies [4, eqs.(3.64),(3.67)]

$$\bar{T}(\xi, \eta, t) \cdot (\xi \hat{x} + \eta \hat{y} + \zeta \hat{z}) = 0, \quad \xi^2 + \eta^2 < c^{-2} \tag{3.41}$$

$$\bar{T}(\xi, \eta, t) \cdot (\xi \hat{x} + \eta \hat{y}) + |\zeta| \mathcal{H} \bar{T}(\xi, \eta, t) \cdot \hat{z} = 0, \quad \xi^2 + \eta^2 > c^{-2} \tag{3.42}$$

where $\mathcal{H}$ is the Hilbert transform given in (3.37). Since $\nabla \times \bar{E} = -\mu \frac{\partial}{\partial t} \bar{H}$ it follows that the Radon transform for the magnetic field is [4, eqs.(3.69),(3.70)]

$$\bar{T}_H(\xi, \eta, t) = \frac{1}{\mu}(\xi \hat{x} + \eta \hat{y} + \zeta \hat{z}) \times \bar{T}(\xi, \eta, t), \quad \xi^2 + \eta^2 < c^{-2} \tag{3.43}$$

$$\bar{T}_H(\xi, \eta, t) = \frac{1}{\mu}(\xi \hat{x} + \eta \hat{y}) \times \bar{T}(\xi, \eta, t) + \frac{|\zeta|}{\mu} \hat{z} \times \mathcal{H} \bar{T}(\xi, \eta, t), \quad \xi^2 + \eta^2 > c^{-2} \tag{3.44}$$

and thus the Radon transform of the magnetic field is determined from the Radon transform of the electric field.

The electric field in the half space $z > 0$ can be calculated by the formula [4, eq.(3.62)]

$$\bar{E}(\bar{r}, t) = -\frac{1}{2\pi} \int_{-\infty}^{+\infty} \int_{-\infty}^{+\infty} \int_{-\infty}^{+\infty} \Phi^B(\bar{r}, t - t', \xi, \eta) \frac{\partial^2}{\partial t'^2} \bar{T}(\xi, \eta, t') dt' d\xi d\eta, \quad z > 0 \tag{3.45}$$

where Φ^B is the time-domain plane wave (3.20). The time-domain far field is given by the simple expression [4, eq.(3.71)]

$$\bar{E}(\bar{r}, t) \sim \frac{\cos \theta}{cr} \frac{\partial}{\partial t} \bar{T}(c^{-1} \cos \phi \sin \theta, c^{-1} \sin \phi \sin \theta, t - r/c), \quad 0 \le \theta < \pi/2. \tag{3.46}$$

Defining the time-domain far-field pattern $\bar{\mathcal{F}}(\theta, \phi, t)$ for the test antenna such that the far electric field is $\bar{E}(\bar{r}, t) \sim \bar{\mathcal{F}}(\theta, \phi, t - r/c)/r$ one finds from (3.46) that

$$\bar{\mathcal{F}}(\theta, \phi, t) = \frac{\cos \theta}{c} \frac{\partial}{\partial t} \bar{T}(c^{-1} \cos \phi \sin \theta, c^{-1} \sin \phi \sin \theta, t), \quad 0 \le \theta < \pi/2. \tag{3.47}$$

Having summarized all the Radon transform formulas for the electric field, we now turn to the problem of deriving the time-domain probe-corrected formulas. As in Section 2.2 for the frequency-domain electromagnetic field, the vector output of the probe is defined by (2.16) as a vector sum of the scalar output in two orientations. The time-domain dyadic receiving

characteristic $\overline{\overline{R}}_p(\xi,\eta,t)$ is defined such that when the incident field is $\Phi^B(\bar{r},t-t',\xi,\eta)\bar{e}(\xi,\eta)$, with $\bar{e}(\xi,\eta)$ satisfying (3.41) and (3.42), the vector output of the probe is given by

$$\bar{b}_p(\bar{r}_0,t) = \overline{\overline{R}}_p(\xi,\eta,t-\xi x_0 - \eta y_0)\cdot\bar{e}(\xi,\eta), \quad \bar{r}_0 = x_0\hat{x} + y_0\hat{y} \qquad (3.48)$$

when the probe is located at $\bar{r}_0$.

The time-domain dyadic receiving characteristic is simply the inverse Fourier transform of the corresponding frequency-domain dyadic and because the vector output of the probe has only x and y components, it can be written as

$$\overline{\overline{R}}_p(\xi,\eta,t) = \hat{x}\bar{R}_p^x(\xi,\eta,t) + \hat{y}\bar{R}_p^y(\xi,\eta,t). \qquad (3.49)$$

From the expansion (3.45) of the field radiated by the test antenna it is seen that when the probe is illuminated by this field and is located at $\bar{r}_0$, its total output is given by

$$\bar{b}_p(\bar{r}_0,t) = -\frac{1}{2\pi}\int_{-\infty}^{+\infty}\int_{-\infty}^{+\infty}\int_{-\infty}^{+\infty}\overline{\overline{R}}_p(\xi,\eta,t-t'-\xi x_0 - \eta y_0)\cdot\frac{\partial^2}{\partial t'^2}\bar{T}(\xi,\eta,t')dt'd\xi d\eta \quad (3.50)$$

which is the electromagnetic analog to the acoustic formula (3.25). The time-domain inverse receiving characteristic $\overline{\overline{R}}_p^{-1}(\xi,\eta,t)$ is simply the inverse Fourier transform of the frequency-domain inverse receiving characteristic given in (2.24)

$$\overline{\overline{R}}_p^{-1}(\xi,\eta,t) = \int_{-\infty}^{+\infty}\frac{\hat{k}(\xi,\eta)\times\left[\bar{R}_{p\omega}^y(\omega\xi,\omega\eta)\hat{x} - \bar{R}_{p\omega}^x(\omega\xi,\omega\eta)\hat{y}\right]}{\hat{k}(\xi,\eta)\cdot\left[\bar{R}_{p\omega}^y(\omega\xi,\omega\eta)\times\bar{R}_{p\omega}^x(\omega\xi,\omega\eta)\right]}e^{-i\omega t}d\omega \qquad (3.51)$$

where the unit vector $\hat{k}(\xi,\eta) = c\xi\hat{x} + c\eta\hat{y} + c\zeta\hat{z}$. It does not seem possible, in general, to express the inverse time-domain receiving characteristic directly in terms of the x and y components, $\bar{R}_p^x(\xi,\eta,t)$ and $\bar{R}_p^y(\xi,\eta,t)$. According to (2.21), for all (ξ,η) the dyadic receiving characteristic and its inverse satisfy

$$\int_{-\infty}^{+\infty}\overline{\overline{R}}_p^{-1}(\xi,\eta,t-t')\cdot\overline{\overline{R}}_p(\xi,\eta,t')dt' = 4\pi^2\delta(t)\left[\hat{\theta}(\xi,\eta)\hat{\theta}(\xi,\eta) + \hat{\phi}(\xi,\eta)\hat{\phi}(\xi,\eta)\right] \qquad (3.52)$$

where $\hat{\theta}(\xi,\eta)$ and $\hat{\phi}(\xi,\eta)$ are time-independent unit vectors given by

$$\hat{\theta}(\xi,\eta) = \frac{\zeta\xi}{c\sqrt{\xi^2+\eta^2}}\hat{x} + \frac{\zeta\eta}{c\sqrt{\xi^2+\eta^2}}\hat{y} - \frac{\sqrt{\xi^2+\eta^2}}{c}\hat{z} \qquad (3.53)$$

and

$$\hat{\phi}(\xi,\eta) = -\frac{\eta}{\sqrt{\xi^2+\eta^2}}\hat{x} + \frac{\xi}{\sqrt{\xi^2+\eta^2}}\hat{y}. \qquad (3.54)$$

Taking the inverse Fourier transform of the probe-corrected formula (2.25) one obtains the following three alternative time-domain probe-corrected formulas

$$\bar{T}(\xi,\eta,t) = \frac{1}{(2\pi)^3}\int_{-\infty}^{+\infty}\overline{\overline{R}}_p^{-1}(\xi,\eta,t')\cdot\int_{-\infty}^{+\infty}\int_{-\infty}^{+\infty}\bar{b}_p(\bar{r}_0,t-t'+\xi x_0 + \eta y_0)dx_0 dy_0 dt' \quad (3.55)$$

26

$$\bar{T}(\xi,\eta,t) = \frac{1}{(2\pi)^3} \int_{-\infty}^{+\infty} \int_{-\infty}^{+\infty} \int_{-\infty}^{+\infty} \overline{\overline{R}}_p^{-1}(\xi,\eta,t-t'+\xi x_0 + \eta y_0) \cdot \bar{b}_p(\bar{r}_0,t')dx_0 dy_0 dt' \quad (3.56)$$

and

$$\bar{T}(\xi,\eta,t) = \frac{1}{(2\pi)^3} \int_{-\infty}^{+\infty} \int_{-\infty}^{+\infty} \int_{-\infty}^{+\infty} \overline{\overline{R}}_p^{-1}(\xi,\eta,t-t'+\xi x_0 + \eta y_0) \cdot \bar{b}_p(\bar{r}_0,t')dt' dx_0 dy_0 \quad (3.57)$$

where $\bar{r}_0 = x_0\hat{x} + y_0\hat{y}$. As for the acoustic field, equation (3.57) may be the most attractive for measurement purposes since the inner time integral can be calculated at each scan point $\bar{r}_0$ for the desired values of (ξ,η,t). Thus, one would not have to store the values of the vector output of the probe over time to calculate the Radon transform of the electric field radiated by the test antenna.

3.2.1   Formulas for Time-Derivative Probes

If the electromagnetic probe is a so-called D-dot probe [10], [11], [14], [15] its output from an incoming plane wave is proportional to the time derivative of the plane-wave field and the frequency-domain receiving characteristic is

$$\overline{\overline{R}}_{p\omega}(\omega\xi,\omega\eta) = -\frac{i\omega}{2\pi}\overline{\overline{Q}}_p(\xi,\eta) = -\frac{i\omega}{2\pi}\left[\hat{x}\bar{Q}_p^x(\xi,\eta) + \hat{y}\bar{Q}_p^y(\xi,\eta)\right] \quad (3.58)$$

where the angularly dependent function $\overline{\overline{Q}}_p(\xi,\eta)$ is independent of the frequency. (Note from (2.32) and (2.33) that a reciprocal elementary electric dipole probe is a D-dot probe.) With this receiving characteristic, the time-domain probe-corrected formula reduces to

$$\frac{\partial}{\partial t}\bar{T}(\xi,\eta,t) = \frac{1}{2\pi}\overline{\overline{Q}}_p^{-1}(\xi,\eta) \cdot \int_{-\infty}^{+\infty} \int_{-\infty}^{+\infty} \bar{b}_p(\bar{r}_0,t+\xi x_0 + \eta y_0)dx_0 dy_0 \quad (3.59)$$

where $\overline{\overline{Q}}_p^{-1}(\xi,\eta)$ is found from (2.24) to be

$$\overline{\overline{Q}}_p^{-1}(\xi,\eta) = \frac{\hat{k}(\xi,\eta) \times \left[\bar{Q}_p^y(\xi,\eta)\hat{x} - \bar{Q}_p^x(\xi,\eta)\hat{y}\right]}{\hat{k}(\xi,\eta) \cdot \left[\bar{Q}_p^y(\xi,\eta) \times \bar{Q}_p^x(\xi,\eta)\right]}, \quad \hat{k}(\xi,\eta) = c\xi\hat{x} + c\eta\hat{y} + c\zeta\hat{z}. \quad (3.60)$$

Combining the expression (3.59) for the time derivative of the Radon transform of the near-field with the expression (3.47) for the far-field pattern shows that the far-field pattern is given by

$$\bar{\mathcal{F}}(\theta,\phi,t) = \frac{\cos\theta}{2\pi c}\overline{\overline{Q}}_p^{-1}(c^{-1}\cos\phi\sin\theta, c^{-1}\sin\phi\sin\theta) \cdot \int_{-\infty}^{+\infty} \int_{-\infty}^{+\infty} \bar{b}_p(\bar{r}_0,t+\hat{r}\cdot\bar{r}_0/c)dx_0 dy_0$$
$$(3.61)$$

where $0 \le \theta < \pi/2$. Thus, for D-dot probes the probe-corrected formula simplifies so that only the calculation of a double integral is needed to find the Radon transform $\bar{T}$ or the far-field pattern $\bar{\mathcal{F}}$.

3.2.2 Formulas for Reciprocal Probes

Finally we consider the reciprocal probe and derive time-domain reciprocity relations between the transmitting and receiving characteristics of the probe, using the Fourier transform along with frequency-domain reciprocity relations. We define the time-domain transmitting characteristic $\bar{T}_p^{\delta x}(\xi, \eta, t)$ of the probe, when its reference line is parallel to the x axis, to be the Radon transform (3.40) of the field radiated by the probe into the half space $z < 0$ when it is located at $\bar{r}_0 = \bar{0}$ and is fed by the delta-function input signal $a_p(t) = 2\pi\delta(t)$.

The frequency-domain reciprocity relation (2.27) shows that for all real ω

$$\bar{R}_{p\omega}^x(\xi\omega, \eta\omega) = \begin{cases} \frac{\zeta}{\mu\eta_0}\bar{T}_{p\omega}^{\delta x}(-\xi\omega, -\eta\omega), & \xi^2 + \eta^2 < c^{-2} \\ \frac{\omega}{|\omega|}\frac{\zeta}{\mu\eta_0}\bar{T}_{p\omega}^{\delta x}(-\xi\omega, -\eta\omega), & \xi^2 + \eta^2 > c^{-2} \end{cases} \tag{3.62}$$

which by use of the inverse Fourier transform gives the time-domain reciprocity relation

$$\bar{R}_p^x(\xi, \eta, t) = \begin{cases} \frac{\zeta}{\mu\eta_0}\bar{T}_p^{\delta x}(-\xi, -\eta, t), & \xi^2 + \eta^2 < c^{-2} \\ \frac{|\zeta|}{\mu\eta_0}\mathcal{H}\bar{T}_p^{\delta x}(-\xi, -\eta, t), & \xi^2 + \eta^2 > c^{-2} \end{cases} \tag{3.63}$$

where $\mathcal{H}$ is the Hilbert transform given in (3.37). A similar result holds when the reference line of the probe is parallel to the y axis. Inserting the expression (3.63) for $\bar{R}_p^x$ and the corresponding expression for $\bar{R}_p^y$ into (3.51) gives a formula for the inverse receiving characteristic in terms of the transmitting characteristics in the two orientations.

3.3 Time-Domain Sampling Theorem and Numerical Far-Field Calculations

In this section we will consider only the special cases where the output of the probe, due to an incoming plane wave, is proportional to the time derivative of that plane-wave field. These cases are of practical interest because such probes actually are used for time-domain measurements [10], [11], [14], [15]. Two different computation schemes, each of which numerically calculates the time-domain far-field pattern from sampled near-field data, will be presented. The first is the frequency-domain computation scheme, which is based on the frequency-domain probe-corrected formulas derived in Chapter 2. The second is the time-domain computation scheme, which is based on the time-domain probe-corrected formulas derived in Chapter 3.

3.3.1 Frequency-Domain Computation Scheme

This computation scheme is similar to the non-probe-corrected scheme presented in [4, sec.4.1] and consists of the following three steps: (1) use the Fourier transform to calculate the frequency-domain output of the probe from the measured time-domain output of

the probe, (2) calculate the frequency-domain far field from the frequency-domain output of the probe, and (3) use the inverse Fourier transform to calculate the time-domain far field from the frequency-domain far field. This scheme makes use of well-known frequency-domain probe-corrected formulas (2.8) or (2.25), sampling theorems, and the fast Fourier transform (FFT). The formulas for the discrete version of this scheme to calculate the time-domain acoustic far-field pattern $\mathcal{F}$ are easily found from the non-probe-corrected formulas [4, sec.4.1, eqs.(4.5)-(4.7)]. We summarize the probe-corrected formulas for the acoustic field below.

Assume that the output of the probe is bandlimited so that $b_{p\omega}$ can be set equal to zero for $|\omega| > \omega_{max}$ and assume that $b_p(\bar{r}_0, t)$ begins at some time t_0 (which may depend on the position $\bar{r}_0$ in the scan plane) and ends approximately at a time that can be expressed as $t_0 + (N_\omega - 1)\Delta t$ where $\Delta t = \pi/\omega_{max}$. Then the frequency-domain output of the probe can be calculated from

$$b_{p\omega}(\bar{r}_0) = \frac{1}{2\pi} \sum_{m=0}^{N_\omega - 1} b_p(\bar{r}_0, t_0 + m\Delta t) e^{i\omega(t_0 + m\Delta t)} \Delta t, \quad |\omega| < \omega_{max}. \quad (3.64)$$

The frequency-domain far-field pattern can be found from the probe-corrected formulas (2.8) and (2.5). With the receiving characteristic given by (3.16) the discrete form of this formula becomes

$$\mathcal{F}_\omega(\theta, \phi) = a_{0\omega}\mathcal{F}_{0\omega}(\theta, \phi) = \frac{\cos\theta}{2\pi c Q_p(c^{-1}\cos\phi\sin\theta, c^{-1}\sin\phi\sin\theta)}$$
$$\cdot \sum_{m=-N_x}^{N_x} \sum_{n=-N_y}^{N_y} b_{p\omega}(\bar{r}_{0mn}) e^{-i\omega\hat{r}\cdot\bar{r}_{0mn}/c} \Delta x_0 \Delta y_0 \quad (3.65)$$

where $\bar{r}_{0mn} = m\Delta x_0\hat{x} + n\Delta y_0\hat{y}$ is a sampling point on the scan plane. The sample spacing $\Delta x_0 = \Delta y_0 = \lambda_{min}/2 = \pi c/\omega_{max}$ is required by the frequency-domain sampling theorem [1, fig.10], while N_x and N_y are integers that determine the size of the scan plane, and $\hat{r} = \hat{x}\cos\phi\sin\theta + \hat{y}\sin\phi\sin\theta + \hat{z}\cos\theta$ is the direction to the far-field observation point. Now that the frequency-domain far-field pattern is calculated, the time-domain far-field pattern is found from the inverse Fourier transform

$$\mathcal{F}(\theta, \phi, t) = \sum_{m=-N_\omega/2}^{N_\omega/2} \mathcal{F}_{m\Delta\omega}(\theta, \phi) e^{-im\Delta\omega t} \Delta\omega, \quad \Delta\omega = \frac{2\omega_{max}}{N_\omega} \quad (3.66)$$

by means of the sampling theorem if the far field $\mathcal{F}(\theta, \phi, t)$ has about the same duration as the output of the probe. If the time duration of the far field is longer than that of the output of the probe, one must decrease the frequency sample spacing $\Delta\omega$ by increasing N_ω. The numerical example given at the end of this section shows that the duration of the calculated far-field pattern, in general, depends not only on the near field but also on the size of the scan plane. This is because the artificial edges of the scan plane produce a diffracted field that will make the time duration of the far-field pattern calculated from (3.66) longer than that of the exact far-field pattern.

3.3.2 Time-Domain Computation Scheme

This computation scheme is similar to the non-probe-corrected scheme presented in [4, sec.4.2] and uses the direct formulas (3.18) or (3.61), which give the time-domain far-field pattern directly in terms of the time-domain output of the probe. The discrete version of the formula (3.18) to calculate the acoustic far-field pattern $\mathcal{F}$ is similar to the non-probe-corrected formula [4, sec.4.2, eq.(4.11)], and can be found by Fourier transforming (3.65) to get

$$
\mathcal{F}(\theta, \phi, t) = \frac{\cos\theta}{2\pi c Q_p(c^{-1}\cos\phi\sin\theta, c^{-1}\sin\phi\sin\theta)}
$$
$$
\cdot \sum_{m=-N_x}^{N_x} \sum_{n=-N_y}^{N_y} b_p(\bar{r}_{0mn}, t + \hat{r}\cdot\bar{r}_{0mn}/c)\Delta x_0 \Delta y_0. \tag{3.67}
$$

3.3.3 Comparisons of the Two Computation Schemes

The comparison given in [4, sec.4.4] of the non-probe-corrected computation schemes also applies to the probe-corrected ones. Specifically, when the far fields of electrically large radiators are calculated for all times and all angles of observation, the FFT makes the frequency-domain computation scheme much faster than the time-domain computation scheme. When only part of the far field is calculated, the difference in computer time for the two computation schemes becomes smaller and the time-domain computation scheme becomes more advantageous because of its simplicity. The time-domain computation scheme is much easier to use than the frequency-domain computation scheme and it is consequently the more attractive scheme when one is not concerned with the amount of computer time it takes to perform the far-field calculations. Furthermore, the calculated far-field pattern has an extended time duration because of the finite scan plane and to avoid aliasing, this extended duration has to be taken into account when the frequency-domain computation scheme is used. The time-domain computation scheme does not make use of the Fourier transform and thus does not encounter this aliasing problem.

As pointed out in Section 3.1, planar time-domain near-field antenna measurements, unlike single-frequency near-field measurements, have the capability of eliminating finite scan errors. This makes it possible to determine the far-field pattern of broadbeam antennas from planar time-domain measurements, as will be demonstrated in the following example.

3.3.4 Numerical Example

The probe-corrected formula (3.18), and its discrete version (3.67), will now be verified numerically by using the time-domain computation scheme to calculate the far-field pattern of an acoustic point source with Gaussian time dependence. The near-field data used in this

computation are obtained by measuring the near field of the point source with a nonideal probe.

The acoustic point source with Gaussian time dependence is located at $\bar{r}_1 = -d\hat{z}$ and its radiated field is given by

$$\Phi^G(\bar{r}, t) = \frac{f(t - |\bar{r} + d\hat{z}|/c)}{4\pi|\bar{r} + d\hat{z}|}, \quad f(t) = e^{-4t^2/\tau^2} \tag{3.68}$$

where τ and d are positive constants. The near-field data are obtained by using a probe whose receiving characteristic is in the form (3.31), that is, the output of the probe due to the incoming plane wave Φ^B is proportional to the time derivative of the incoming plane wave Φ^B. The angularly dependent function $Q_p(\xi, \eta)$ is chosen to be $\cos\theta$, where θ is the angle between the propagation direction of the plane wave and the z axis. Since the propagation direction of the plane wave is given by $\hat{k} = \xi c\hat{x} + \eta c\hat{y} + \zeta c\hat{z}$, the angularly dependent function is

$$Q_p(\xi, \eta) = c\zeta = \begin{cases} |\sqrt{1 - \xi^2 c^2 - \eta^2 c^2}|, & \xi^2 + \eta^2 < c^{-2} \\ i|\sqrt{\xi^2 c^2 + \eta^2 c^2 - 1}|, & \xi^2 + \eta^2 > c^{-2} \end{cases} \tag{3.69}$$

To calculate the double summation (3.67) for the far-field pattern, we have to know the output of the probe at each scan point on the scan plane. Since the receiving characteristic of the probe is defined in terms of plane waves we have to expand the acoustic point-source field in terms of plane waves in order to determine the output of the probe.

We start by writing the acoustic point-source field (3.68) in terms of the Fourier integral

$$\Phi^G(\bar{r}, t) = \int_{-\infty}^{+\infty} \frac{f_\omega e^{ik|\bar{r} + d\hat{z}|}}{4\pi|\bar{r} + d\hat{z}|} e^{-i\omega t} d\omega \tag{3.70}$$

where $f_\omega = \tau(4\sqrt{\pi})^{-1} e^{-\omega^2 \tau^2/16}$ is the spectrum of the Gaussian time function $f(t)$ in (3.68). The reason we write the acoustic field in this form is that we can now make use of the identity [4, eq.(2.29)] to show that

$$\frac{f_\omega e^{ik|\bar{r} + d\hat{z}|}}{4\pi|\bar{r} + d\hat{z}|} = \frac{if_\omega}{8\pi^2} \int_{-\infty}^{+\infty} \int_{-\infty}^{+\infty} \frac{1}{\gamma} e^{i[k_x x + k_y y + \gamma(z+d)]} dk_x dk_y \tag{3.71}$$

which gives the frequency-domain point-source field in terms of plane waves. The plane-wave spectrum for the point-source field (3.70) is then seen from (3.71) and (2.1) to be

$$T_{0\omega}(k_x, k_y) = \frac{if_\omega}{4\pi\gamma} e^{i\gamma d}. \tag{3.72}$$

Then (2.7) shows that the frequency-domain output of the probe is given by

$$b_{p\omega}(\bar{r}_0) = \frac{if_\omega}{4\pi} \int_{-\infty}^{+\infty} \int_{-\infty}^{+\infty} \frac{R_{p\omega}(k_x, k_y)}{\gamma} e^{i(k_x x_0 + k_y y_0 + \gamma d)} dk_x dk_y, \quad z_0 = 0 \tag{3.73}$$

where $R_{p\omega}$ is the frequency-domain receiving characteristic of the special time-derivative probe found from (3.16) and (3.69) to be

$$R_{p\omega}(k_x, k_y) = -\frac{i\omega Q_p(\xi, \eta)}{2\pi} = -\frac{ic\omega\zeta}{2\pi} = -\frac{ic\gamma}{2\pi}. \tag{3.74}$$

Inserting this expression for the receiving characteristic of the probe into (3.73) and making use of (3.71), one finds that the frequency-domain output of the probe is given by

$$b_{p\omega}(\bar{r}_0) = -\frac{cf_\omega}{4\pi}\frac{\partial}{\partial d}\frac{e^{ik|\bar{r}_0 + d\hat{z}|}}{|\bar{r}_0 + d\hat{z}|}. \tag{3.75}$$

Note that this expression could also have been given in terms of a partial derivative with respect to z. However, since $z = 0$ on the scan plane it is more convenient to write it in terms of the distance d between the point source and the scan plane. Taking the inverse Fourier transform of (3.75) shows that the time-domain output of the probe is simply

$$b_p(\bar{r}_0, t) = -c\frac{\partial}{\partial d}\Phi^G(\bar{r}_0, t) \tag{3.76}$$

where Φ^G is the Gaussian acoustic point-source field (3.68). We have now shown that the output of the probe equals $-c$ times the partial derivative with respect to d (or z) of the point-source field. This result could also have been obtained by using the formulas of [7] where receiving antennas are described as linear differential operators. When the distance between the probe and the point source is large, (3.76) shows that the output of the probe is $b_p(\bar{r}_0, t) \approx \cos\theta\frac{\partial}{\partial t}\Phi^G(\bar{r}_0, t)$ where θ is the angle between the z axis and the vector going from the point source to the point $\bar{r}_0$ on the scan plane. This result is explained by noting that the point-source field at a position $\bar{r}_0$ in the far field consists of a plane wave propagating in the direction given by θ, and the output of the special probe equals $\cos\theta$ times the time derivative of an incident plane-wave field.

Having calculated the output of the probe we use (3.18) to find the following expression for the far-field pattern of the test antenna

$$\mathcal{F}(\theta, \phi, t) = -\frac{1}{2\pi}\int_{-\infty}^{+\infty}\int_{-\infty}^{+\infty}\frac{\partial}{\partial d}\Phi^G(\bar{r}_0, t + \hat{r}\cdot\bar{r}_0/c)dx_0dy_0, \quad 0 \le \theta < \pi/2. \tag{3.77}$$

The discrete version of (3.77) useful for computation is obtained from (3.67) as

$$\mathcal{F}(\theta, \phi, t) = -\frac{1}{2\pi}\sum_{m=-N_x}^{N_x}\sum_{n=-N_y}^{N_y}\frac{\partial}{\partial d}\Phi^G(\bar{r}_{0mn}, t + \hat{r}\cdot\bar{r}_{0mn}/c)\Delta x_0\Delta y_0, \quad 0 \le \theta < \pi/2. \tag{3.78}$$

If probe correction had been neglected, the far-field pattern would have been given by the right side of (3.77) or (3.78) divided by $\cos\theta$. Thus, probe correction can be neglected only if $\cos\theta \approx 1$.

Let us now show the computed far-field pattern of the Gaussian acoustic point source obtained from the near-field formula (3.78). In the previous report [4, sec.4.3] it was shown
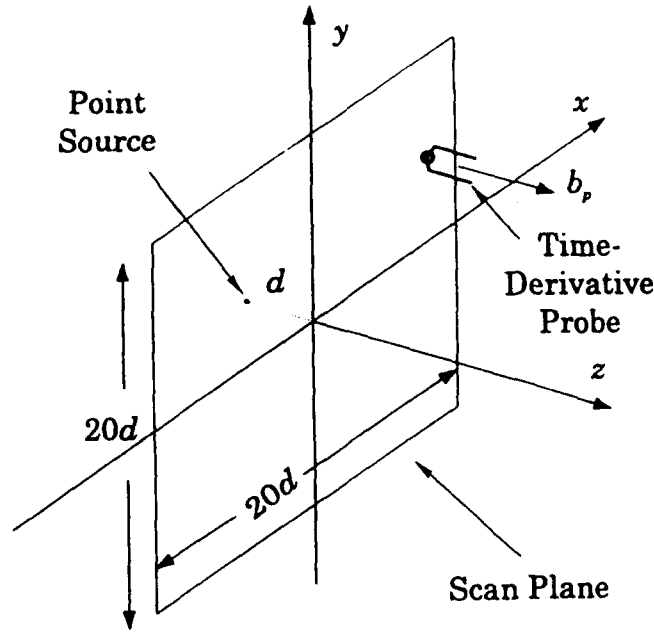
32

Figure 3.5: Gaussian point source measured on a finite scan plane with a time-derivative probe.

that the maximum effective frequency in the acoustic field (3.68) is $\omega_{max} \simeq 12/\tau$ and thus the shortest wave length is $\lambda_{min} = 2\pi c/\omega_{max} \simeq c\tau/2$. For the numerical calculations we choose $d = 2\lambda_{min} \simeq c\tau$. To satisfy the requirements of the sampling theorem [4, sec.4.2], the near field is sampled with spatial sample spacing $\Delta x_0 = \Delta y_0 = \lambda_{min}/2 \simeq c\tau/4$. The far-field pattern will be calculated for $(\theta, \phi) = (45°, 0)$ and the scan plane is chosen to be a square of sidelength $20d$, which is large enough to avoid the problems of the interference between the correct field and the erroneous field for this angle of observation. The erroneous field is due to the edges of the scan plane and has been discussed in [4, sec.4.4]. With this size of the scan plane and this observation direction, the erroneous signal ends approximately 20.5τ after the correct signal. Thus, the duration of the far-field pattern calculated from (3.77) is approximately 23τ whereas the duration of the exact far-field pattern is only 2.5τ. See Figure 3.5 for a picture of the scanning geometry.

Figure 3.6 shows the far-field pattern calculated for $(\theta, \phi) = (45°, 0)$ in three different ways: (a) is the exact Gaussian far-field pattern; (b) is the far-field pattern calculated without probe correction by inserting the output of the probe (3.76) as if it were the measured near field Φ^G, into [4, eq.(4.11)]; and (c) is the far-field pattern calculated by the probe-corrected formula (3.78).

The curve (a), which is exact, has the Gaussian wave form and is only significantly nonzero on the interval $-0.5\tau < t < 2.0\tau$. The curve (b), which is obtained without probe correction,
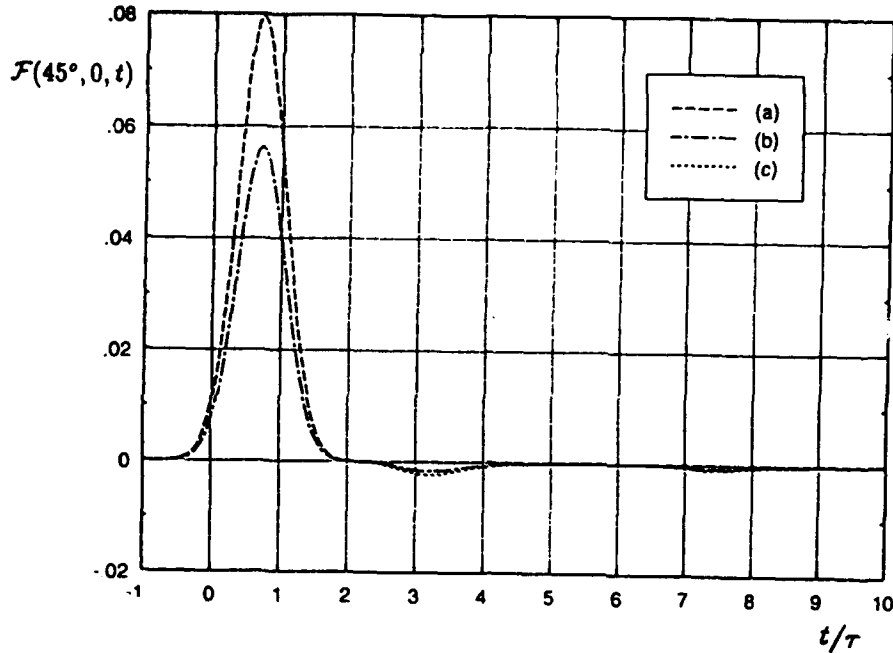
33

Figure 3.6: Values of the far-field pattern $\mathcal{F}(45^\circ, 0, t)$. (a) exact; (b) without probe correction; (c) with probe correction.

is clearly in error even on the interval where the exact far-field pattern is nonzero. In fact, it equals $\cos 45^\circ \approx 0.707$ times the probe-corrected value given by the curve (c). The curve (c), which is obtained from the probe-corrected formula (3.78), cannot be distinguished from the exact curve on the interval $-\tau < t < 2.4\tau$. Because of the finite size of the scan plane the curves (b) and (c) are erroneous (negative) on parts of the interval from $t = 2.4\tau$ to $t = 23\tau$ (the end of the erroneous signal ($t = 23\tau$) is found by determining the time after which the field is identically zero on the finite scan plane [4, sec.4.4]). However, the erroneous parts for the curve (c) do not overlap with the interval where the exact far-field pattern is nonzero so the curve (c) is an excellent approximation to the exact far-field pattern. The curve (b) obtained without probe-correction is seen to be a very poor approximation to the exact far-field pattern. Probe correction is therefore required to get an accurate far-field pattern when this special time-derivative probe with $\cos \theta$ angular dependence is used. Furthermore, it is demonstrated that time-domain planar near-field measurements can be used to accurately determine the far-field pattern of broadbeam antennas that cannot be accurately measured in the frequency domain because of the errors introduced by the finite scan plane.

34

References

[1] Yaghjian, A.D. (1986) An overview of near-field antenna measurements, *IEEE Trans. Antennas Propagat.* **34**:30-45.

[2] Kerns, D.M. (1963) Analytical techniques for the correction of near-field antenna measurements made with an arbitrary but known measuring antenna, in *Abstracts of URSI-IRE Meeting*, Washington, DC, April-May 1963:6-7.

[3] Kerns, D.M. (1982) *Plane-Wave Scattering-Matrix Theory of Antennas and Antenna-Antenna Interactions*, NBS Monograph 162.

[4] Hansen, T.B. and Yaghjian, A.D. (1993) *Formulation of time-domain planar near-field measurements without probe correction*, Rome Laboratory Technical Report RL-TR-93-210, ADA276380.

[5] Kerns, D.M. (1975) Scattering-matrix description and near field measurements of electroacoustic transducers, *J. Acoust. Soc. Am.*, **57**, (2):497-507.

[6] Yaghjian, A.D. (1975) Generalized or adjoint reciprocity relations for electroacoustic transducers, *J. Res. B*, **79B**:17-39.

[7] Yaghjian, A.D. and Wittmann, R.C. (1985) The receiving antenna as a linear differential operator: Application to spherical near-field scanning, *IEEE Trans. Antennas Propagat.* **33**:1175-1185.

[8] Yaghjian, A.D. (1992) Antenna coupling and near-field sampling in plane-polar coordinates, *IEEE Trans. Antennas Propagat.* **40**:304-312.

[9] van Bladel, J. (1964) *Electromagnetic Fields*, New York: McGraw-Hill.

[10] Kanda, M. (1983) Time domain sensors for radiated impulsive measurements, *IEEE Trans. Antennas Propagat.* **31**:438-444.

[11] Ziolkowski, R.W. (1992) Properties of electromagnetic beams generated by ultra-wide bandwidth pulse-driven arrays, *IEEE Trans. Antennas Propagat.* **40**:888-905.

[12] Deans, S.R. (1983) *The Radon Transform and Some of Its Applications*, New York: Wiley.

[13] Morse, P.M. and Feshbach, H. (1953) *Methods of Theoretical Physics*, New York: McGraw-Hill.

[14] Baum, C.E., Breen, E.L., Giles, J.C., O'Neill, J. and Sower, G.D. (1978) Sensors for electromagnetic pulse measurements both inside and away from nuclear source regions, *IEEE Trans. Antennas Propagat.* **26**:22-35.

[15] Hill, D.A. (1986) *Far-field transient response of an antenna from near-field data*, NBS In-House Report, NBSIR 86-3063.

MISSION

OF

ROME LABORATORY

Mission. The mission of Rome Laboratory is to advance the science and technologies of command, control, communications and intelligence and to transition them into systems to meet customer needs. To achieve this, Rome Lab:

    a. Conducts vigorous research, development and test programs in all applicable technologies;

    b. Transitions technology to current and future systems to improve operational capability, readiness, and supportability;

    c. Provides a full range of technical support to Air Force Materiel Command product centers and other Air Force organizations;

    d. Promotes transfer of technology to the private sector;

    e. Maintains leading edge technological expertise in the areas of surveillance, communications, command and control, intelligence, reliability science, electro-magnetic technology, photonics, signal processing, and computational science.

The thrust areas of technical competence include: Surveillance, Communications, Command and Control, Intelligence, Signal Processing, Computer Science and Technology, Electromagnetic Technology, Photonics and Reliability Sciences.